

AD-A090 031

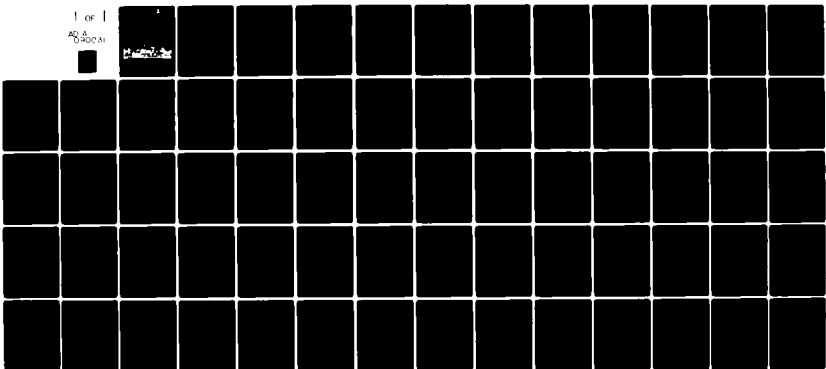
ARMY ENGINEER WATERWAYS EXPERIMENT STATION VICKSBURG--ETC F/8 8/11
CALCULATION OF GROUND SHOCK MOTION PRODUCED BY AIRBURST EXPLOSI--ETC(U)
SEP 80 J R BRITT
WES/MP/SL-80-12


UNCLASSIFIED

NL

1 of 1

AD A
090031



END

DATE

FILED

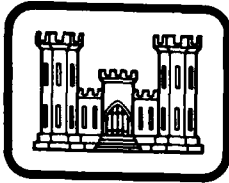
11-80

DTIC

K

LEVEL

2



MISCELLANEOUS PAPER SL-80-12

CALCULATION OF GROUND SHOCK MOTION PRODUCED BY AIRBURST EXPLOSIONS USING CAGNIARD ELASTIC PROPAGATION THEORY

by

J. R. Britt

Structures Laboratory
U. S. Army Engineer Waterways Experiment Station
P. O. Box 631, Vicksburg, Miss. 39180

September 1980

Final Report

Approved For Public Release; Distribution Unlimited

AD A090031

OTIC
LECTE
OCT 8 1980



Prepared for Assistant Secretary of the Army (R&D)
Washington, D. C. 20310

Under Project No. 4A161101A91D

DDC FILE COPY

80 10 7 077

**Destroy this report when no longer needed. Do not return
it to the originator.**

**The findings in this report are not to be construed as an official
Department of the Army position unless so designated
by other authorized documents.**

**The contents of this report are not to be used for
advertising, publication, or promotional purposes.
Citation of trade names does not constitute an
official endorsement or approval of the use of
such commercial products.**

Unclassified

SECURITY CLASSIFICATION OF THIS PAGE (When Data Entered)

REPORT DOCUMENTATION PAGE		READ INSTRUCTIONS BEFORE COMPLETING FORM
1. REPORT NUMBER Miscellaneous Paper SL-80-12	2. GOVT ACCESSION NO. AD-A090031	3. RECIPIENT'S CATALOG NUMBER
6. TITLE (and Subtitle) CALCULATION OF GROUND SHOCK MOTION PRODUCED BY AIRBURST EXPLOSIONS USING CAGNIARD ELASTIC PROPAGATION THEORY.	5. TYPE OF REPORT & PERIOD COVERED 9. Final report, No. 78 - Jun 81	
	6. PERFORMING ORG. REPORT NUMBER	
7. AUTHOR(s) James R. Britt	8. CONTRACT OR GRANT NUMBER(s)	
9. PERFORMING ORGANIZATION NAME AND ADDRESS U. S. Army Engineer Waterways Experiment Station Structures Laboratory P. O. Box 631, Vicksburg, Miss. 39180	10. PROGRAM ELEMENT, PROJECT, TASK AREA & WORK UNIT NUMBERS Project No. 4A161101A91D	
11. CONTROLLING OFFICE NAME AND ADDRESS Assistant Secretary of the Army (R&D) Washington, D. C. 20310	12. REPORT DATE 11. Sep 80 12. 67	
14. MONITORING AGENCY NAME & ADDRESS (if different from Controlling Office)	13. NUMBER OF PAGES 63	
	15. SECURITY CLASS. (of this report) Unclassified	
15a. DECLASSIFICATION/DOWNGRADING SCHEDULE		
16. DISTRIBUTION STATEMENT (of this Report) Approved for public release; distribution unlimited.		
17. DISTRIBUTION STATEMENT (of the abstract entered in Block 20, if different from Report)		
18. SUPPLEMENTARY NOTES		
19. KEY WORDS (Continue on reverse side if necessary and identify by block number) Air blast waves Ground motion Cagniard's method Ground shock Computer codes Spherical waves Elastic waves Surface explosions		
20. ABSTRACT (Continue on reverse side if necessary and identify by block number) This report describes a study which used elastic wave propagation theory to predict ground motion produced by airburst explosions of spherical charges. The air-earth environment was treated as three elastic layers (air, soil, and rock) separated by plane parallel boundaries. The explosion was approximated by a point source in an elastic fluid. The exact, closed form integral solutions of L. Cagniard for the reflection and refraction of spherical waves in elastic solids were extended to model the ground shock propagation (continued)		

DD FORM 1473 / EDITION OF 1 NOV 65 IS OBSOLETE

Unclassified

SECURITY CLASSIFICATION OF THIS PAGE (When Data Entered)

411 415

Unclassified

SECURITY CLASSIFICATION OF THIS PAGE(When Data Entered)

20. ABSTRACT (continued).

in layered earth. Nonlinear empirical airblast arrival time and pressure source waveform formulae were developed and were used as source inputs for the elastic calculations.

A computer code CAGGS was developed to evaluate the integral solutions to produce ground shock particle velocity waveforms. Calculations were compared with experimental records, for soil-soil, soil-rock, and rock sites. At gage locations where the airblast overpressures are less than approximately 40 psi for weak soils and over 100 psi for strong rocks, these comparisons show generally good agreement in the important characteristics amplitude, pulse shape, and arrival times. The results of the study indicate that the CAGGS code can be a valuable tool for studying the basic characteristics and effects of the controlling parameters of ground shock in layered earth media.

Unclassified

SECURITY CLASSIFICATION OF THIS PAGE(When Data Entered)

PREFACE

The study described in this report was performed during the period November 1978-June 1980, under Project No. 4A161101A91D and was sponsored by the Assistant Secretary of the Army (R&D) under the In-House Laboratory Independent Research (ILIR) Program.

The report was prepared by Mr. James R. Britt of the Explosion Effects Division (EED), Structures Laboratory (SL), U. S. Army Engineer Waterways Experiment Station (WES), Vicksburg, Mississippi. The CAGGS computer code developed in this study was an outgrowth of bottom reflection codes developed by the author and Dr. Hans G. Snay at the Naval Surface Weapons Center (NSWC), formerly the Naval Ordnance Laboratory. Copies of these codes for use at WES were obtained through the aid of Mrs. Norma Holland of NSWC. The author is indebted to Mr. James L. Drake, EED, who provided stimulating discussions on the theoretical and experimental aspects of the study and who assisted in the technical editing of the report.

The work was done under the general direction of Mr. L. F. Ingram, Chief, EED, and Mr. W. J. Flathau, Assistant Chief, SL, and Mr. Bryant Mather, Chief, SL.

COL John L. Cannon, CE, and COL Nelson P. Conover, CE, were Commanders and Directors of WES during the performance of this work. Technical Director was Mr. F. R. Brown.

Approved For	
APR 1981	1
F111 118	11
Approved	
J. L. F. Ingram	
Signature	
Date	
Part	

A

CONTENTS

	<u>Page</u>
CHAPTER 1 INTRODUCTION-----	4
CHAPTER 2 THEORY-----	6
2.1 Theoretical Background-----	6
2.2 Equations of Motion-----	6
2.3 Boundary and Initial Conditions-----	8
2.4 Problem Solution in Laplace Transform Domain-----	9
2.5 Derivation of Generalized Reflection and Transmission Coefficients-----	13
2.6 Derivation of the Source Factor-----	17
2.7 A Ray Numbering Scheme for 3-Layer Media-----	18
2.8 Example of the Construction of Transformed Solutions-----	19
2.9 Inversion of the Transformed Solutions-----	21
2.10 Change of Integration Variable From ω to u -----	23
2.11 Arrival Times-----	24
2.12 The Change of Integration Variable From u to w -----	26
2.13 Solutions for Velocity Components-----	27
2.14 Solutions for Stress Components-----	29
2.15 Limiting Values of the Potential Solutions at $t = t_{2q}$ and $r = 0$ -----	31
CHAPTER 3 THE CAGGS CODE-----	34
3.1 General Description-----	34
3.2 Code Inputs and Outputs-----	34
3.3 Numerical Integration Procedure-----	37
3.4 Modeling the Airblast Waveform-----	39
3.5 Approximation of the Airblast with a Point Source-----	45
CHAPTER 4 COMPARISON OF CALCULATED AND MEASURED PARTICLE VELOCITY WAVEFORMS-----	47
4.1 Selection of Test Series-----	47
4.2 Calculations for CENSE 1-----	47
4.3 Calculations for CENSE 2-----	49
4.4 Calculations for CENSE 3-----	49
CHAPTER 5 CONCLUSIONS AND RECOMMENDATIONS-----	59
REFERENCES-----	61

LIST OF TABLES

Tables

1	Characteristic parameters of rays $q = 1$ to 12-----	20
2	Sample printout of a CAGGS calculation-----	35
3	Explosive test series used in the airblast model-----	42

LIST OF FIGURES

<u>Figure</u>		<u>Page</u>
1	Model for airburst explosions over layered earth media-----	4
2	Typical airblast waveform-----	41
3	Comparison of particle velocity calculations with CENSE 1 measurements at 48-ft range-----	48
4	Comparison of particle velocity calculations with CENSE 1 measurements at 36-ft range-----	50
5	Comparison of particle velocity calculations with CENSE 2 measurements at 67-ft range-----	51
6	Comparison of particle velocity calculations with CENSE 2 measurements at 43-ft range-----	52
7	Comparison of particle velocity calculations with CENSE 2 measurements at 32-ft range-----	53
8	Comparison of particle velocity calculations with CENSE 3 measurements at 56-ft range-----	55
9	Comparison of particle velocity calculations with CENSE 3 measurements at 32-ft range-----	56
10	Particle velocity calculations for 12-ft and infinitely thick soil layers-----	57

CONVERSION FACTORS, INCH-POUND TO METRIC (SI)
UNITS OF MEASUREMENT

Inch-pound units of measurement used in this report can be converted to metric (SI) units as follows:

<u>Multiply</u>	<u>By</u>	<u>To Obtain</u>
feet	0.3048	metres
feet per second	0.3048	metres per second
feet per millisecond	304.8	metres per second
pounds (mass)	0.45359237	kilograms
tons (mass)	907.1847	kilograms
pounds (force) per square inch	6.894757	kilopascals
kilotons (nuclear equivalent of TNT)	4.20×10^{12}	joules

CALCULATION OF GROUND SHOCK MOTION PRODUCED BY
AIRBURST EXPLOSIONS USING CAGNIARD
ELASTIC PROPAGATION THEORY

CHAPTER 1

INTRODUCTION

This report describes a study which used elastic wave propagation theory to predict and analyze ground motions produced by near surface airburst explosions. The primary objectives of the study were to develop a calculational capability using the exact Cagniard (1962) elastic formulation and to determine the practical applications of the method.

In this study the air-earth environment was modeled as three homogeneous elastic layers--air, soil and rock--separated by plane parallel boundaries as illustrated in Figure 1. The air was treated as

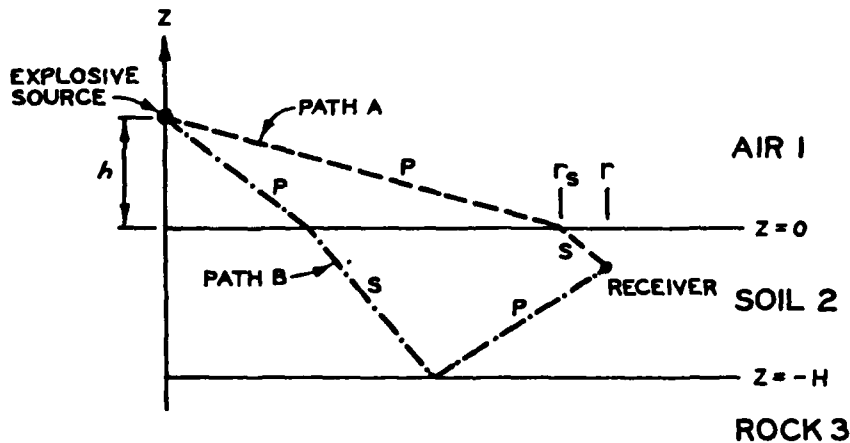


Figure 1 Model for airburst explosions over layered earth media.

an elastic fluid, while the soil and rock were treated as elastic solids. An airburst explosion of spherical charges was approximated by a point source located on the axis of symmetry. Nonlinear empirical airblast arrival time and overpressure waveform formulae were developed to

specify the source characteristics for elastic calculations.

The exact closed form integral solutions of Cagniard for the reflection and refraction of spherical waves in elastic solids were adapted and extended to model the ground shock propagation in a layered earth. In this formulation the particle motion is obtained as a sum of components propagated along rays or paths (such as shown in Figure 1) associated with distinct wave arrivals. Calculations using the Cagniard procedure were used previously successfully to predict the reflection of underwater explosion shock waves from the ocean bottom Rosenbaum (1956), Britt (1969, 1970), Britt and Snay (1971), Snay and Britt (1973).¹ The theoretical analysis and computer code development for the ground shock calculations were extensions of this bottom reflection study.

In the following sections solutions of the wave propagation equations for layered elastic media are derived using the Cagniard approach. Much of the theoretical development can be found in the literature. Hence, the goal of this report is to present only the basic steps of the solution procedure and to bring together all the equations needed for the ground shock calculations in a form tailored to the problem. The CAGGS (Cagniard Ground Shock) computer code developed for evaluating these solutions to obtain particle velocity histories is discussed, and comparisons of calculated and measured waveforms are presented and analyzed.

¹ Classified reference. Bibliographic material for the classified reference will be furnished to qualified agencies upon request.

CHAPTER 2

THEORY

2.1 THEORETICAL BACKGROUND

The geometry of the ground shock model is shown in Figure 1 for the 3-layer case used in the CAGGS computer code. Development of the theory will be given in a general form applicable to an arbitrary number of layers. Because of the symmetry, axisymmetric equations of motion in a cylindrical coordinate system are appropriate. The source is located on the z-axis at the point (0,h) in the fluid half-space denoted "air." The observer (receiver or gage) position is (r,z) in the finite layer of thickness H denoted "soil." Both the layer and the underlying "rock" half-space are modeled as elastic solids so that the labels "soil" and "rock" are arbitrary.

The solutions of the elastic wave propagation equations were obtained using the methods developed by Cagniard (1939, 1962) for the reflection and refraction of elastic waves at an interface between two elastic solids. The solutions were extended to layered media by Spencer (1960, 1965), Pekeris, et al. (1965), Abramovici and Alterman (1965), and Abramovici (1970). Additional information on work using the Cagniard approach and other elastic wave solutions in layered media is given in the books by Ewing, Jardetzky and Press (1957) and Brekhovskikh (1960) and the summary papers of Pao, et al. (1971, 1977) and Britt (1969). Examples of the more recent literature are Abramovici (1978), Abramovici and Gal-Ezer (1978, 1979), and Pao, et al. (1979).

2.2 EQUATIONS OF MOTION

Using a notation similar to Cagniard (1962), scalar potentials X_j and U_j can be defined for an elastic solid medium j such that the radial and vertical velocity components \dot{x}_{rj} and \dot{x}_{zj} are given by

$$\dot{x}_{rj} = \frac{\partial X_j}{\partial r} - \frac{\partial U_j}{\partial z} \quad (2.2.1)$$

$$\ell_{zj} = \frac{\partial X_j}{\partial z} + \frac{\partial U_j}{\partial r} + \frac{U_j}{r} \quad (2.2.2)$$

These potentials are to satisfy the elastic wave propagation equations in cylindrical coordinates

$$\nabla^2 X_j = \frac{1}{c_{pj}^2} \frac{\partial^2 X_j}{\partial t^2} \quad (2.2.3)$$

$$\nabla^2 U_j - \frac{U_j}{r^2} = \frac{1}{c_{sj}^2} \frac{\partial^2 U_j}{\partial t^2} \quad (2.2.4)$$

where

$$\nabla^2 = \frac{\partial^2}{\partial r^2} + \frac{\partial^2}{\partial z^2} + \frac{1}{r} \frac{\partial}{\partial r}$$

t denotes time, and c_{pj} and c_{sj} are the wave propagation speeds of compressional (P) and shear (S) waves, respectively. For fluid layers c_{sj} and U_j are zero. The subscript j refers to the layers.

The stress components for density ρ_j can be expressed as follows:

normal stresses

$$(\tau_{zz})_j = \rho_j \left[\left(1 - 2 \frac{c_{sj}^2}{c_{pj}^2} \right) \frac{\partial^2 X_j}{\partial t^2} + 2 c_{sj}^2 \frac{\partial \ell_{zj}}{\partial z} \right] \quad (2.2.5)$$

$$(\tau_{rr})_j = \rho_j \left[\left(1 - 2 \frac{c_{sj}^2}{c_{pj}^2} \right) \frac{\partial^2 X_j}{\partial t^2} + 2 c_{sj}^2 \frac{\partial \ell_{rj}}{\partial r} \right] \quad (2.2.6)$$

$$(\tau_{\phi\phi})_j = \rho_j \left[\left(1 - 2 \frac{c_{sj}^2}{c_{pj}^2} \right) \frac{\partial^2 X_j}{\partial t^2} + 2 c_{sj}^2 \frac{\ell_{rj}}{r} \right] \quad (2.2.7)$$

tangential stresses

$$(\tau_{r\phi})_j = 0 \quad (2.2.8)$$

$$(\tau_{rz})_j = \rho_j c_{sj}^2 \left(\frac{\partial \ell_{rj}}{\partial z} + \frac{\partial \ell_{zj}}{\partial r} \right) \quad (2.2.9)$$

$$(\tau_{z\phi})_j = 0 \quad (2.2.10)$$

mean normal stress

$$(\tau_{\text{mean}})_j = \rho_j \left(1 - \frac{4}{3} c_{sj}^2 / c_{pj}^2 \right) \frac{\partial^2 X_j}{\partial t^2} \quad (2.2.11)$$

In a fluid the tangential stresses all vanish and the normal stresses are equal to the mean normal stress given by

$$(\tau_{\text{mean}})_j = -P_j = \rho_j \frac{\partial^2 X_j}{\partial t^2} \quad (2.2.12)$$

where P_j is the pressure.

2.3 BOUNDARY AND INITIAL CONDITIONS

Assuming perfect coupling at the interfaces the boundary conditions of the problem are continuity of displacement and stress normal and tangential to the interfaces. At an interface $z = z_{jk}$ separating media j and k these conditions are

$$\ell_{zj} = \ell_{zk} \quad (2.3.1)$$

$$\ell_{rj} = \ell_{rk} \quad (2.3.2)$$

$$(\tau_{zz})_j = (\tau_{zz})_k \quad (2.3.3)$$

$$(\tau_{rz})_j = (\tau_{rz})_k \quad (2.3.4)$$

In order that the media be at rest before the source is initiated, the potentials X_j and U_j and their derivatives must vanish at $t = 0$ and in the limit as $R = [r^2 + (h - z)^2]^{1/2}$ goes to infinity.

The source at $(0, h)$ is taken into account by imposing the

condition: for $z \rightarrow h$ and $r \rightarrow 0$ the solution tends to that corresponding to a point pressure (or mean normal stress) source located in medium m

$$P_m = -\frac{\rho_m}{R} \frac{\partial^2 X_o(t - R/c_{pm})}{\partial t^2} = \frac{1}{R} P_o(t - R/c_{pm})^* \quad (2.3.5)$$

where $X_o(t - R/c_{pm}) = 0$ and $P_o(t - R/c_{pm}) = 0$ for $t < R/c_{pm}$. Solutions for other types of sources are available in the literature, but the pressure source is most appropriate for modeling an airburst explosion. In future work a combination of various source types should be considered.

2.4 PROBLEM SOLUTION IN LAPLACE TRANSFORM DOMAIN

In this chapter we begin solving the boundary value problem using the Cagniard procedure. Briefly, in this method one obtains a solution by Laplace transform techniques. Then through a series of changes of integration variables and paths the solution is inverted by inspection back to the time domain. The basic steps and results are presented here. Cagniard (1962) and the other references can be consulted for the rigorous mathematical details.

The first step is to Laplace transform with respect to time, t , the propagation equations (2.2.3) and (2.2.4), equations for the potentials, velocities, stresses, and the boundary conditions. Let the transform variable be s and denote a transformed function by placing a bar over the function symbol. For the given initial conditions the propagation equations become

$$v^2 \bar{X}_j = \frac{s^2}{c_{pj}^2} \bar{X}_j \quad (2.4.1)$$

$$v^2 \bar{U}_j - \frac{\bar{U}_j}{r^2} = \frac{s^2}{c_{sj}^2} \bar{U}_j \quad (2.4.2)$$

* Note that the dimensions of X_o and P_o are RX_m and RP_m , respectively.

The source condition (2.3.5) becomes

$$\bar{P}_m = -\rho_m s^2 \left(\bar{X}_o e^{-sR/c_{pm}} \right) = \frac{1}{R} \bar{P}_o e^{-sR/c_{pm}} \quad (2.4.3)$$

which can be written

$$\bar{P}_m = s \bar{P}_o \left(\frac{1}{sR} e^{-sR/c_{pm}} \right) \quad (2.4.4)$$

The term in parenthesis is the transform of the spherical step waveform

$$P_{\text{step}} = \frac{1}{R} H(t - R/c_{pm}) \quad (2.4.5)$$

where

$$H(t - R/c_{pm}) = \begin{cases} 0 & \text{for } t < R/c_{pm} \\ 1 & \text{for } t \geq R/c_{pm} \end{cases} \quad (2.4.6)$$

is the unit step function.

Applying the convolution theorem for Laplace transforms to (2.4.4) and (2.4.5) yields

$$\bar{P}_m = \int_0^t P'_o(t - \lambda) P_{\text{step}}(\lambda) d\lambda \quad (2.4.7)$$

The same argument can also be applied to the $\bar{X}_o e^{-sR/c_{pm}}$ factor of equation (2.4.3). This result suggests expressing the transformed potentials as

$$\bar{X}_j = s \bar{X}_o \bar{X}_j^{\text{step}} \quad (2.4.8)$$

$$\bar{U}_j = s \bar{X}_o \bar{U}_j^{\text{step}} \quad (2.4.9)$$

where \bar{X}_j^{step} and \bar{U}_j^{step} are solutions for a spherical point source $\frac{1}{R} H(t - R/c_{pm})$. The solutions for an arbitrary time function

$X_0(t - R/c_{pm})$ are then obtained from

$$X_j = \int_0^t X'_0(t - \lambda) X_j^{\text{step}}(\lambda) d\lambda \quad (2.4.10)$$

$$U_j = \int_0^t X'_0(t - \lambda) U_j^{\text{step}}(\lambda) d\lambda \quad (2.4.11)$$

Here $\frac{1}{R} X_0$ is the source function. But in the equations for particle velocity and stress it will be advantageous to use the original pressure source function $\frac{1}{R} P_0(t - R/c_{pm})$ which is proportional to the second time derivative of X_0 in (2.3.5).

The significance of the above representations is that solutions can be found for step sources from which solutions for an arbitrary time dependence can be obtained by the convolution integrals. The solutions X_j^{step} and U_j^{step} will be treated in the following sections. For simplicity of notation the superscript "step" will be omitted, except when necessary for clarity, and it will be understood that the convolutions must be performed for a specified source function.

Transformed solutions in any of the layers can be written in the form

$$\begin{aligned} \bar{X}_j = & \int_0^\infty a_{pj}(u) \exp(s\alpha_{pj}z) J_0(\text{sur}) du \\ & + \int_0^\infty b_{pj}(u) \exp(-s\alpha_{pj}z) J_0(\text{sur}) du \end{aligned} \quad (2.4.12)$$

$$\begin{aligned} \bar{U}_j = & \int_0^\infty a_{sj}(u) \exp(s\alpha_{sj}z) J'_0(\text{sur}) du \\ & + \int_0^\infty b_{sj}(u) \exp(-s\alpha_{sj}z) J'_0(\text{sur}) du \end{aligned} \quad (2.4.13)$$

where $\alpha_{pj} = \left(u^2 + c_{pj}^{-2}\right)^{1/2}$, $\alpha_{sj} = \left(u^2 + c_{sj}^{-2}\right)^{1/2}$, and $J_0(\text{sur})$ is the Bessel function of the first kind of order zero. The functions a and b are to be determined from the boundary conditions. The terms containing a_{pj} and a_{sj} represent P and S waves, respectively, traveling in the negative z direction. Similarly, the b_{pj} and b_{sj} terms correspond to waves traveling in the positive direction.

The transform of the step source can be put in a similar form using the Sommerfeld integral derived in Ewing, et al. (1957)

$$\frac{1}{sR} \exp(-sR/c_{pm}) = \int_0^{\infty} J_0(\text{sur}) \exp(-s\alpha_{pm}|h-z|) \frac{u \, du}{\alpha_{pm}} \quad (2.4.14)$$

The direct solution for the coefficients a and b is very complicated even for the 3-layer case and results in very involved formulae. (See Abramovici and Alterman (1965) for example.) An alternative approach is the generalized ray path concept introduced by Spencer (1960, 1965). It was shown that the potentials \bar{X}_j and \bar{U}_j can be built up from terms which represent distinct arrivals or rays in the form

$$\bar{X}_j = \sum_q \bar{X}_{jq} = \sum_q \int_0^{\infty} C_q(u) \exp[-s(\sum_k \alpha_k d_k)] J_0(\text{sur}) du \quad (2.4.15)$$

$$\bar{U}_j = \sum_q \bar{U}_{jq} = \sum_q \int_0^{\infty} C_q(u) \exp[-s(\sum_k \alpha_k d_k)] J_0'(\text{sur}) du \quad (2.4.16)$$

where q is an identifier of the ray, $C_q(u)$ contains factors representing the source and the generalized reflection and transmission coefficients for each interface encounter. The subscript k is used symbolically to identify segments of the ray q , and d_k is the vertical projection of the k^{th} segment. If a segment is in medium m , then α_k denotes α_{pm} and α_{sm} for P and S waves, respectively. A ray represents a term in \bar{X}_j or \bar{U}_j if the last segment which joins to the receiver is a P wave or S wave, respectively.

Spencer (1960) derived the method of generalized rays by first considering the interactions at a single interface for incident P and S waves. These interactions can be identified with two letters: the first denoting the type (P or S) of the incident wave and the second the type of the reflected or transmitted wave. There are then four combinations PP, PS, SP and SS for both reflections and transmissions for a total of eight possible interface interactions for which coefficients must be determined. Once derived the formulae can be used at any interface by inserting the applicable wave speeds and densities.

Starting at the source, rays can be drawn representing all the possible types of paths which join the source to the receiver. The appropriate coefficients (derived in the next section) are then included in $C_q(u)$ for each interface encounter of the ray. By considering the ray segment beginning at the source which has no interface contact, the "source factor" (derived in Section 2.6) to be included in $C_q(u)$ can be determined.

The arrival time (derived in Section 2.11) along each ray depends on the wave speeds and the number and lengths of segments. At a given time only those rays which "have arrived" must be considered.

2.5 DERIVATION OF GENERALIZED REFLECTION AND TRANSMISSION COEFFICIENTS

In this section equations are derived for the generalized reflection and transmission coefficients. Consider the case of waves incident only from medium j onto medium k . Let the interface separating media j and k be $z = 0$. Substitute the solutions in the form of (2.4.12) and (2.4.13) into transformed versions of the boundary conditions (2.3.1)-(2.3.4) using (2.2.1), (2.2.2), (2.2.5)-(2.2.10) to express displacement and stress components in terms of the potentials. Assuming that medium j is above k , the terms containing a_{pj} and a_{sj} represent the incident waves and hence $b_{pk} = b_{sk} = 0$. The resulting equations can be put in a form similar to that used by Ewing, et al. (1957) for plane wave reflection using the notation

$$Q = \rho_k c_{sk}^2 / \rho_j c_{sj}^2 \quad (2.5.1)$$

$$A_i = 2u^2 + c_{si}^{-2} \quad \text{for } i = j \text{ or } k \quad (2.5.2)$$

$$L_1 = (QA_k - 2u^2) c_{sj}^2 \quad (2.5.3)$$

$$L_2 = \frac{u}{\alpha_{sj}} (QA_k - A_j) c_{sj}^2 \quad (2.5.4)$$

$$L_3 = \frac{\alpha_{pk}}{\alpha_{pj}} (A_j - 2Qu^2) c_{sj}^2 \quad (2.5.5)$$

$$L_4 = 2u\alpha_{pk} (1 - Q) c_{sj}^2 \quad (2.5.6)$$

$$M_1 = 2u\alpha_{sk} (1 - Q) c_{sj}^2 \quad (2.5.7)$$

$$M_2 = \frac{\alpha_{sk}}{\alpha_{sj}} (A_j - 2u^2Q) c_{sj}^2 \quad (2.5.8)$$

$$M_3 = \frac{u}{\alpha_{pj}} (QA_k - A_j) c_{sj}^2 \quad (2.5.9)$$

$$M_4 = L_1 \quad (2.5.10)$$

After some manipulation the boundary conditions yield equations as follows:

$$L_1 a_{pk} + M_1 a_{sk} = a_{pj} + b_{pj} \quad (2.5.11)$$

$$L_2 a_{pk} + M_2 a_{sk} = a_{sj} - b_{sj} \quad (2.5.12)$$

$$L_3 a_{pk} + M_3 a_{sk} = a_{pj} - b_{pj} \quad (2.5.13)$$

$$L_4 a_{pk} + M_4 a_{sk} = a_{sj} + b_{sj} \quad (2.5.14)$$

Setting $a_{pj} = 0$, a_{sj} is the only incident term and equations (2.5.11)-(2.5.14) can be solved for the generalized reflection coefficients K and transmission coefficients T for an incident S wave. Define

$$D = (L_1 + L_3)(M_2 + M_4) - (L_2 + L_4)(M_1 + M_3) \quad (2.5.15)$$

to obtain

$$K_{jk}^{sp} = \frac{b_{pj}}{a_{sj}} = 2(L_3M_1 - L_1M_3)/D \quad (2.5.16)$$

$$K_{jk}^{ss} = \frac{b_{sj}}{a_{sj}} = [(L_2 - L_4)(M_1 + M_3) - (L_1 + L_3)(M_2 - M_4)]/D \quad (2.5.17)$$

$$T_{jk}^{sp} = \frac{a_{pk}}{a_{sj}} = -2(M_1 + M_3)/D \quad (2.5.18)$$

$$T_{jk}^{ss} = \frac{a_{sk}}{a_{sj}} = 2(L_1 + L_3)/D \quad (2.5.19)$$

where the superscripts denote the types of waves before and after the interface interaction, and the subscripts denote waves incident from medium j onto medium k .

Incident P waves can be considered by setting $a_{sj} = 0$. The resulting coefficients are

$$K_{jk}^{pp} = \frac{b_{pj}}{a_{pj}} = [(L_1 - L_3)(M_2 + M_4) - (L_2 + L_4)(M_1 - M_3)]/D \quad (2.5.20)$$

$$K_{jk}^{ps} = \frac{b_{sj}}{a_{pj}} = 2(L_4M_2 - L_2M_4)/D \quad (2.5.21)$$

$$T_{jk}^{PP} = \frac{a_{pk}}{a_{pj}} = 2(M_2 + M_4)/D \quad (2.5.22)$$

$$T_{jk}^{PS} = \frac{a_{sk}}{a_{pj}} = -2(L_2 + L_4)/D \quad (2.5.23)$$

Since both media j and k are solids, coefficients K_{kj} and T_{kj} for waves incident from media k can be obtained by simply interchanging the subscripts in the above equations. In the case that one medium is a fluid and one is a solid this symmetry does not hold, but the coefficients can be obtained by taking the limit as c_s of the fluid goes to zero.

Denote the fluid medium by j and the solid k . After taking the limit $c_{sj} \rightarrow 0$, the coefficients above can be simplified by defining

$$f = \rho_j / \rho_k \quad (2.5.24)$$

$$D_{jk} = \alpha_{pj} \left(A_k^2 - 4u^2 \alpha_{pk} \alpha_{sk} \right) + f \alpha_{pk} c_{sk}^{-4} \quad (2.5.25)$$

The resulting coefficients for waves incident from the fluid are

$$K_{jk}^{PP} = \left[\alpha_{pj} \left(A_k^2 - 4u^2 \alpha_{pk} \alpha_{sk} \right) - f \alpha_{pk} c_{sk}^{-4} \right] / D_{jk} \quad (2.5.26)$$

$$T_{jk}^{PP} = 2f \alpha_{pj} A_k c_{sk}^{-2} / D_{jk} \quad (2.5.27)$$

$$T_{jk}^{PS} = 4uf \alpha_{pj} \alpha_{pk} c_{sk}^{-2} / D_{jk} \quad (2.5.28)$$

For waves incident from the solid medium k the coefficients are

$$K_{kj}^{sp} = -4u\alpha_{pj}\alpha_{sk}A_k/D_{jk} \quad (2.5.29)$$

$$K_{kj}^{ss} = -\left[\alpha_{pj}\left(A_k^2 + 4u^2\alpha_{pk}\alpha_{sk}\right) + f\alpha_{pk}c_{sk}^{-4}\right]/D_{jk} \quad (2.5.30)$$

$$K_{kj}^{pp} = -\left[\alpha_{pj}\left(A_k^2 + 4u^2\alpha_{pk}\alpha_{sk}\right) - f\alpha_{pk}c_{sk}^{-4}\right]/D_{jk} \quad (2.5.31)$$

$$K_{kj}^{ps} = -4u\alpha_{pj}\alpha_{pk}A_k/D_{jk} \quad (2.5.32)$$

$$T_{kj}^{pp} = 2\alpha_{pk}A_k c_{sk}^{-2}/D_{jk} \quad (2.5.33)$$

$$T_{kj}^{sp} = 4u\alpha_{pk}\alpha_{sk}c_{sk}^{-2}/D_{jk} \quad (2.5.34)$$

The coefficients for shear components in the fluid are all zero.

For the case of two fluid media the coefficients simplify to

$$K_{jk}^{pp} = (\alpha_{pj} - f\alpha_{pk})/(\alpha_{pj} + f\alpha_{pk}) \quad (2.5.35)$$

$$T_{jk}^{pp} = 2f\alpha_{pj}/(\alpha_{pj} + f\alpha_{pk}) \quad (2.5.36)$$

Again there is symmetry for waves incident from medium k , and now all coefficients involving shear waves are zero.

2.6 DERIVATION OF THE SOURCE FACTOR

The source factor in $C_q(u)$ can be determined by equating the

integral representation (2.4.14) for a P wave source with the $q = 0$ (no interface encounters) term of (2.4.15)

$$\int_0^{\infty} C_0(u) \exp(-s\alpha_{pm} d_0) J_0(sur) du \quad (2.6.1)$$

$$= \int_0^{\infty} J_0(sur) \exp(-s\alpha_{pm} |h - z|) \frac{u du}{\alpha_{pm}}$$

Equating expressions inside the integrals gives

$$C_0 \exp(-s\alpha_{pm} d_0) = \frac{u}{\alpha_{pm}} \exp(-s\alpha_{pm} |h - z|) \quad (2.6.2)$$

Let

$$d_0 = |h - z| \quad (2.6.3)$$

and

$$C_0 = u/\alpha_{pm} \quad (2.6.4)$$

Thus $C_q(u)$ for a P wave source can be expressed in the form

$$C_q(u) = \frac{u}{\alpha_{pm}} \Pi_q(KT) \quad (2.6.5)$$

where $\Pi_q(KT)$ denotes a product of reflection and transmission coefficients for each interface encounter of ray q .

2.7 A RAY NUMBERING SCHEME FOR 3-LAYER MEDIA

The 3-layer geometry of Figure 1 was used for the ground shock calculations in this report. A simple ray numbering scheme for this case is as follows. First group together rays having the same number of reflections within the layer. Then within each group arrange rays

according to an increasing number of S wave segments. S segments extending the full thickness of the layer are counted higher than segments which cross only part of the layer. This scheme arranges rays within a group according to increasing arrival times for the common situation in which $|z| < H/2$ and $c_s < c_p/2$.

Each ray can be identified by the letters P or S of its segments. The first segment in the fluids is always P and its letter designation will be dropped. The last segment crosses only part of the layer and hence has a value of d_k , vertical projection, which is less than H. The other segments in the layer have $d_k = H$. For calculational efficiency rays having the same $\Sigma \alpha_k d_k$ (and hence the same arrival times) are numbered together and computed with the same integration since all terms in the integrals are the same except for the product of reflection and transmission coefficients $\Pi K T$ in $C_q(u)$. Table 1 lists rays 1 through 12 with the factors $\Sigma \alpha_k d_k$ and the products $\Pi K T$. Note that rays 9 and 10 are degenerate, having two components.

For higher ordered reflections the labels $P^n S^m S$ or $P^n S^m P$ can be used, where n and m denote the number of P and S segments, respectively, crossing the layer. The last letter denotes the type of the last segment. Using this notation the general formula for $\Sigma \alpha_k d_k$ for ray q is


$$\Sigma \alpha_k d_k = h \alpha_{p1} + n H \alpha_{p2} + m H \alpha_{s2} + \begin{pmatrix} -z \\ H + z \end{pmatrix} \times \begin{pmatrix} \alpha_{p2} \\ \alpha_{s2} \end{pmatrix} \quad (2.7.1)$$

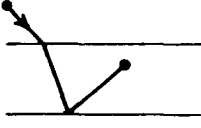
The choice of the upper or lower terms in braces depends on the last segment of the ray. $H + z$ is used if the segment is upward ($n + m$ odd), and $-z$ is used if the segment is downward ($n + m$ even). α_{p2} is used if the last segment is a P wave (q odd), and α_{s2} is used for a S wave (q even).

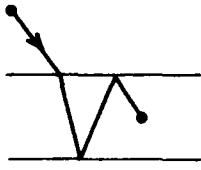
2.8 EXAMPLE OF THE CONSTRUCTION OF TRANSFORMED SOLUTIONS

As an example of how the ray solutions \bar{X}_{jq} and \bar{U}_{jq} are

Table 1. Characteristic parameters of rays $q = 1$ to 12

Path diagram	q	Path type	$\sum \alpha_k d_k$	$\Pi_{k k k} T_k$
	1	P	$\alpha_{p1} h - \alpha_{p2} z$	T_{12}^{pp}
	2	S	$\alpha_{p1} h - \alpha_{s2} z$	T_{12}^{ps}

	3	PP	$\alpha_{p1} h + \alpha_{p2} (2H + z)$	$T_{12}^{pp,pp} K_{23}$
	4	PS	$\alpha_{p1} h + \alpha_{p2} H + \alpha_{s2} (H + z)$	$T_{12}^{pp,ps} K_{23}$
	5	SP	$\alpha_{p1} h + \alpha_{s2} H + \alpha_{p2} (H + z)$	$T_{12}^{ps,sp} K_{23}$
	6	SS	$\alpha_{p1} h + \alpha_{s2} (2H + z)$	$T_{12}^{ps,ss} K_{23}$

	7	PPP	$\alpha_{p1} h + \alpha_{p2} (2H - z)$	$T_{12}^{pp,pp,pp} K_{23} K_{21}$
	8	PPS	$\alpha_{p1} h + \alpha_{p2} (2H) - \alpha_{s2} z$	$T_{12}^{pp,pp,ps} K_{23} K_{21}$
	9	PSP	$\alpha_{p1} h + \alpha_{p2} (H - z) + \alpha_{s2} H$	$T_{12}^{pp,ps,sp} K_{23} K_{21}$
		SPP		$T_{12}^{ps,sp,pp} K_{23} K_{21}$
	10	PSS	$\alpha_{p1} h + \alpha_{p2} H + \alpha_{s2} (H - z)$	$T_{12}^{pp,ps,ss} K_{23} K_{21}$
		SPS		$T_{12}^{ps,sp,ps} K_{23} K_{21}$
	11	SSP	$\alpha_{p1} h - \alpha_{p2} z + \alpha_{s2} (2H)$	$T_{12}^{ps,ss,sp} K_{23} K_{21}$
	12	SSS	$\alpha_{p1} h + \alpha_{s2} (2H - z)$	$T_{12}^{ps,ss,ss} K_{23} K_{21}$

constructed, consider the path B shown in Figure 1 which is denoted $q = 5$ in Table 1. Since the last segment is a P wave in medium 2, this ray represents the term $\bar{X}_{2,5}$. The ray is first transmitted from medium 1 into medium 2 with a coefficient T_{12}^{ps} . The ray is then reflected at the interface $z = -H$ with a coefficient K_{23}^{sp} . Hence, from (2.6.5) we obtain

$$C_5 = \frac{u}{\alpha_{p1}} T_{12}^{ps} K_{23}^{sp} \quad (2.8.1)$$

The vertical projections d_k of the ray are h , H and $H + z$, so that

$$\sum_k \alpha_k d_k = \alpha_{p1} h + \alpha_{s2} H + \alpha_{p2} (H + z) \quad (2.8.2)$$

the solution for the ray is then

$$\begin{aligned} \bar{X}_{2,5} = \int_0^{\infty} \left[\frac{u}{\alpha_{p1}} T_{12}^{ps} K_{23}^{sp} \right] \exp \left\{ -s \left[\alpha_{p1} h \right. \right. \\ \left. \left. + \alpha_{s2} H + \alpha_{p2} (H + z) \right] \right\} J_0(\text{sur}) du \end{aligned} \quad (2.8.3)$$

Solutions for the other rays are built up in the same manner.

2.9 INVERSION OF THE TRANSFORMED SOLUTIONS

General terms of (2.4.15) and (2.4.16) are

$$\bar{X}_{jq} = \int_0^{\infty} C_q(u) \exp \left[-s(\sum_k \alpha_k d_k) \right] J_0(\text{sur}) du \quad (2.9.1)$$

$$\bar{U}_{jq} = \int_0^{\infty} C_q(u) \exp \left[-s(\sum_k \alpha_k d_k) \right] J_0'(\text{sur}) du \quad (2.9.2)$$

These expressions can be inverted using Cagniard's method to obtain the

solution X_{jq} and U_{jq} in the time domain. The first step is to substitute into (2.9.1) and (2.9.2) the integral representations

$$J_0(sur) = \operatorname{Re} \left[\frac{2}{\pi} \int_0^{\pi/2} \exp(-isur \cos \omega) d\omega \right] \quad (2.9.3)$$

$$J'_0(sur) = \operatorname{Im} \left[\frac{2}{\pi} \int_0^{\pi/2} \cos \omega \exp(-isur \cos \omega) d\omega \right] \quad (2.9.4)$$

where Re and Im denote real and imaginary parts, respectively, and $i = \sqrt{-1}$. Rearrange the equations to obtain

$$\bar{X}_{jq} = \int_0^\infty \left\{ \frac{2}{\pi} \operatorname{Re} \int_0^{\pi/2} C_q(u) \exp \left[-s \left(\sum_k \alpha_k d_k + iur \cos \omega \right) \right] d\omega \right\} du \quad (2.9.5)$$

$$\bar{U}_{jq} = \int_0^\infty \left\{ \frac{2}{\pi} \operatorname{Im} \int_0^{\pi/2} C_q(u) \cos \omega \exp \left[-s \left(\sum_k \alpha_k d_k + iur \cos \omega \right) \right] d\omega \right\} du \quad (2.9.6)$$

The next step is the key Cagniard substitution: a change of integration variable from u to t at constant ω defined by

$$t = \sum_k \alpha_k d_k + iur \cos \omega \quad (2.9.7)$$

to give¹

$$\bar{X}_{jq} = \int_0^\infty \left\{ \frac{2}{\pi} \operatorname{Re} \int_0^{\pi/2} C_q(u) \left(\frac{\partial u}{\partial t} \right)_\omega d\omega \right\} \exp(-st) dt \quad (2.9.8)$$

¹ Several rigorous mathematical details have been omitted here. See the references (Cagniard (1962) or Britt (1969) for example) for additional information.

$$\bar{U}_{jq} = \int_0^{\infty} \left\{ \frac{2}{\pi} \operatorname{Im} \int_0^{\pi/2} C_q(u) \left(\frac{\partial u}{\partial t} \right)_{\omega} \cos \omega \, d\omega \right\} \exp(-st) dt \quad (2.9.9)$$

From the definition of the Laplace transform the expressions in braces are the inverse transforms

$$X_{jq} = \frac{2}{\pi} \operatorname{Re} \int_0^{\pi/2} C_q(u) \left(\frac{\partial u}{\partial t} \right)_{\omega} \, d\omega \quad (2.9.10)$$

$$U_{jq} = \frac{2}{\pi} \operatorname{Im} \int_0^{\pi/2} C_q(u) \left(\frac{\partial u}{\partial t} \right)_{\omega} \cos \omega \, d\omega \quad (2.9.11)$$

This completes the essential steps of the potential solutions. The following expresses the equations in forms more suitable for computations.

2.10 CHANGE OF INTEGRATION VARIABLE FROM ω TO u

The fact that u in the integrands of (2.9.10) and (2.9.11) cannot in general be explicitly determined as a function of ω makes the numerical integration of these equations difficult. A change of integration variable from ω to u at constant t produces expressions more amenable to computations

$$X_{jq} = \frac{2}{\pi} \operatorname{Im} \int_{u_1}^{u_2} \frac{C_q(u)}{\gamma} \, du \quad (2.10.1)$$

$$U_{jq} = \frac{-2}{\pi r} \operatorname{Im} \int_{u_1}^{u_2} \frac{C_q(u)}{u\gamma} (t - \sum_k \alpha_k d_k) \, du \quad (2.10.2)$$

where we have defined

$$\gamma = \left[u^2 r^2 + \left(t - \sum_k \alpha_k d_k \right)^2 \right]^{1/2} \quad (2.10.3)$$

and u_1 , corresponding to $\omega = 0$, is the solution in the fourth quadrant of the complex plane having the smallest modulus of

$$t = \sum_k \alpha_k (u_1) d_k + i u_1 r \quad (2.10.4)$$

and u_2 corresponding to $\omega = \pi/2$ is the solution of

$$t = \sum_k \alpha_k (u_2) d_k \quad (2.10.5)$$

The imaginary parts of integrals (2.10.1) and (2.10.2) are symmetric about the real axis and the real parts are anti-symmetric. The integrals from u_1 to u_2 can be replaced by integrals from u_1 to \bar{u}_1 where \bar{u}_1 is the complex conjugate of u_1 . The results are

$$X_{jq} = \frac{1}{i\pi} \int_{u_1}^{\bar{u}_1} \frac{C_q(u) du}{\gamma} \quad (2.10.6)$$

$$U_{jq} = -\frac{1}{i\pi r} \int_{u_1}^{\bar{u}_1} \frac{C_q(u)(t - \sum_k \alpha_k d_k)}{u\gamma} du \quad (2.10.7)$$

2.11 ARRIVAL TIMES

An examination of the integrands above reveals that the integrals are zero before a time t_{1q} which will be determined later. In addition there is a characteristic time $t_{2q} \geq t_{1q}$ which is the maximum value of t for which u_1 from (2.10.4) is a pure imaginary number $u_1 = -iy_2$ for $y_2 > 0$. This time t_{2q} corresponds to the arrival time of a ray satisfying Snell's Law of Refraction. The condition necessary for the

maximum is obtained by applying $\partial t / \partial y_2 = 0$ for $u_1 = -iy_2$ in (2.10.4):

$$\sum d_k / \alpha_k (-iy_{2\max}) - r / y_{2\max} = 0 \quad (2.11.1)$$

This gives

$$t_{2q} = \sum \alpha_k (-iy_{2\max}) d_k + y_{2\max} r \quad (2.11.2)$$

We can identify

$$y_{2\max} = c_k^{-1} \sin \theta_k \quad (2.11.3)$$

where θ_k is the angle the k^{th} segment of the ray makes with the normal to the interface. This equation is really a statement of Snell's law since k ranges over all segments of the ray and $y_{2\max}$ is the same for all k .

We next examine the case in which $t_{1q} < t_{2q}$ as defined by (2.11.2). An inspection of the integrands (2.10.6) and (2.10.7) shows that the integrals are zero until at least one of the square roots becomes imaginary or complex. It can be shown that u_1 and \tilde{u}_1 are zeros of γ which means the potentials are non-zero for $t \geq t_{2q}$. For $t_{1q} < t_{2q}$ to exist, one of the α 's in the integrands must have a zero at a value of $u = iy_1$ such that $y_1 < y_{2\max}$. But it has been shown that $y_{2\max}$ is always less than any of the c_k^{-1} which occur in $\sum \alpha_k d_k$. Hence, y_1 must be the zero of some $\alpha_{pn} = (c_{pn}^{-1} - y_1^2)^{1/2}$ occurring in $C_q(u)$ but not in $\sum \alpha_k d_k$. (Since $c_{pn}^{-1} < c_{sn}^{-1}$, only α_{pn} need be considered.) Denote the minimum such c_{pn}^{-1} as c_{pmin}^{-1} . Thus $t_{1q} < t_{2q}$ occurs if $c_{pmin}^{-1} < y_{2\max}$. With $u_1 = -ic_{pmin}^{-1}$, equation (2.10.4) gives

$$t_{1q} = \sum \alpha_k (ic_{pmin}^{-1}) d_k + c_{pmin}^{-1} r \quad (2.11.4)$$

In the following discussion we generalize this definition of t_{1q} to be the minimum arrival time of ray q , hence if no $c_{pmin}^{-1} < y_{2\max}$ exists, then we set $t_{1q} = t_{2q}$.

2.12 THE CHANGE OF INTEGRATION VARIABLE FROM u TO w

An additional change of integration variables in the potential solutions (2.10.6) and (2.10.7) is advantageous because $\gamma(u)$ is zero at the integration limits u_1 and \bar{u}_1 . It is easily shown that the integrands have singularities which behave like $(u - u_1)^{-1/2}$ and $(\bar{u}_1 - u)^{-1/2}$, except at $t = t_{2q}$ when a logarithmic singularity occurs.

The first step in eliminating the singularity for $t \neq t_{2q}$ is to replace the integration from u_1 to \bar{u}_1 by one in the first quadrant of the complex plane. Using a path of constant real part, $\text{Re}(u_1)$, the calculation can be performed using a real integration variable if we set $u = \text{Re}(u_1) + iy$ to give

$$X_{jq} = \frac{2}{\pi} \int_{y_1}^{y_2} \text{Re} \left[\frac{C_q(u)}{\gamma} \right] dy \quad (2.12.1)$$

$$U_{jq} = \frac{-2}{\pi r} \int_{y_1}^{y_2} \text{Re} \left[C_q(u) \frac{(t - \sum_k d_k)}{u\gamma} \right] dy \quad (2.12.2)$$

where $y_2 = \text{Im}(\bar{u}_1)$ and $y_1 = c_{\text{pmin}}^{-1}$ for $t < t_{2q}$ and $y_1 = 0$ for $t > t_{2q}$.

Next make a change of variable (similar to that used by Longman (1961)) from y to

$$w = (y_2 - y)^{1/2} \quad (2.12.3)$$

or

$$\text{Re}(u) = y = y_2 - w^2 \quad (2.12.4)$$

to give

$$X_{jq} = \frac{4}{\pi} \int_0^{w_1} \operatorname{Re} \left[\frac{C_q(u)}{\gamma} \right] w dw \quad (2.12.5)$$

$$U_{jq} = \frac{-4}{\pi r} \int_0^{w_1} \operatorname{Re} \left[\frac{C_q(u)}{u\gamma} (t - \sum_k \alpha_k d_k) \right] w dw \quad (2.12.6)$$

where $w_1 = (y_2 - y_1)^{1/2}$. Since the quotient w/γ has a finite limit as $w \rightarrow 0$ ($y \rightarrow y_2$), the singularity has been eliminated.

2.13 SOLUTIONS FOR VELOCITY COMPONENTS

In explosion effects research particle velocity (or velocity obtained by integrating acceleration) and stress are usually the quantities measured. Equations for velocity and stress components are best derived by performing the various space and time derivatives on the transformed potential solutions (2.9.1) and (2.9.2) rather than determining the derivatives after inverting these solutions.

Since velocity v is related to the displacement l by $v = dl/dt$, the transform is $\bar{v} = s\bar{l}$ for zero initial displacement. Equations for the transformed velocity components can then be obtained from the transformed displacements by simply multiplying by s . Similarly, the $\partial^2 X_{jq} / \partial t^2$ terms in the stresses have transforms $s^2 \bar{X}_{jq}$.

Denote the P wave contribution to the radial velocity for ray q as v_{rq}^p and the shear wave term v_{rq}^s . Similarly, for the vertical velocity use v_{zq}^p and v_{zq}^s . Let $S_q = +1$ for rays in which the last segment is downward and $S_q = -1$ if the last segment is upward. Velocity components are positive upward and outward. Substitute the transformed potentials (2.9.1) and (2.9.2) into transformed versions of equations (2.2.1) and (2.2.2), and multiply by s to obtain

$$\bar{v}_{rq}^p = s \frac{\partial \bar{X}_{jq}}{\partial r} = s^2 \int_0^{\infty} u C_q(u) \exp[-s \sum_k \alpha_k d_k] J_0'(sur) du \quad (2.13.1)$$

$$\bar{v}_{rq}^s = -s \frac{\partial \bar{U}_{jq}}{\partial z} = -s^2 \int_0^{\infty} \alpha_{sj} S_q C_q(u) \exp[-s \Sigma \alpha_k d_k] J'_0(\text{sur}) du \quad (2.13.2)$$

$$\bar{v}_{zq}^p = s \frac{\partial \bar{X}_{jq}}{\partial z} = s^2 \int_0^{\infty} \alpha_{pj} S_q C_q(u) \exp[-s \Sigma \alpha_k d_k] J_0(\text{sur}) du \quad (2.13.3)$$

$$\bar{v}_{zq}^s = s \left[\frac{\partial \bar{U}_{jq}}{\partial r} + \frac{\bar{U}_{jq}}{r} \right] = -s^2 \int_0^{\infty} u C_q(u) \exp[-s \Sigma \alpha_k d_k] J_0(\text{sur}) du \quad (2.13.4)$$

Note that these equations are solutions for a step wave source from which solutions for an arbitrary potential time variation $X_0(t - R/c_{pm})$ can be obtained by using (2.4.10) and (2.4.11).

The s^2 factors above can be eliminated if a pressure source $P_m = \frac{1}{R} P_0(t - R/c_{pm})$ is used instead of the potential source. By applying equation (2.4.3) which relates \bar{X}_0 and \bar{P}_0 , it is easily seen for a velocity component v that we can define

$$\bar{v} = - \frac{s}{\rho_m} \bar{P}_0 \bar{V} \quad (2.13.5)$$

where \bar{V} is obtained from equations (2.13.1)-(2.13.4) by dropping the s^2 factor up front. Then v is obtained from the convolution

$$v = - \frac{1}{\rho_m} \int_0^t P'_0(t - \lambda) v(\lambda) d\lambda \quad (2.13.6)$$

Note that subscripts and superscripts have been dropped for simplicity.

The \bar{V}_r equations involve $J'_0(\text{sur})$ as in \bar{U}_{jq} and can be inverted in the same manner. Similarly, the \bar{V}_z equations contain $J_0(\text{sur})$ and can be inverted as \bar{X}_{jq} was. The results analogous to (2.12.5) and (2.12.6) are

$$V_{rq}^p = -\frac{4}{\pi r} \int_0^{w_1} \operatorname{Re} \left[\frac{C_q(u)}{\gamma} (t - \Sigma \alpha_k d_k) \right] w dw \quad (2.13.7)$$

$$V_{rq}^s = \frac{4}{\pi r} \int_0^{w_1} \operatorname{Re} \left[\frac{\alpha_{sj} S_q C_q(u)}{u \gamma} (t - \Sigma \alpha_k d_k) \right] w dw \quad (2.13.8)$$

$$V_{zq}^p = \frac{4}{\pi} \int_0^w \operatorname{Re} \left[\frac{\alpha_{pj} S_q C_q(u)}{\gamma} \right] w dw \quad (2.13.9)$$

$$V_{zq}^s = -\frac{4}{\pi} \int_0^w \operatorname{Re} \left[\frac{u C_q(u)}{\gamma} \right] w dw \quad (2.13.10)$$

where $S_q = +1$ or -1 when the last segment of ray q is downward or upward, respectively.

2.14 SOLUTIONS FOR STRESS COMPONENTS

For a pressure source we can obtain step wave response functions Z and Y for the stress components which are analogous to the response V for the velocity components. Then corresponding to (2.13.6) the stress components can be obtained from

$$\tau = -\frac{1}{\rho_m} \int_0^t P'_0(t - \lambda) Z(\lambda) d\lambda - \frac{1}{\rho_m} \int_0^t P_0(t - \lambda) Y(\lambda) d\lambda \quad (2.14.1)$$

where the proper superscripts and subscripts are implied on both sides of the equation. The following stress response functions were derived using the same procedure used for the V functions:

$$Z_{zz}^{pq} = \frac{4}{\pi} \rho_j c_{sj}^2 \int_0^{w_1} \operatorname{Re} \left[\frac{A_j}{\gamma} C_q(u) \right] w dw \quad (2.14.2)$$

$$Z_{zz}^{sq} = -\frac{8}{\pi} \rho_j c_{sj}^2 \int_0^{w_1} \operatorname{Re} \left[\frac{u \alpha_{sj} S_q}{\gamma} C_q(u) \right] w dw \quad (2.14.3)$$

$$Z_{rr}^{pq} = \frac{4}{\pi} \rho_j \int_0^{w_1} \operatorname{Re} \left[\left(1 - 2c_{sj}^2 \alpha_{pj}^2 \right) \frac{C_q(u)}{\gamma} \right] w dw \quad (2.14.4)$$

$$Y_{rr}^{pq} = \frac{8}{\pi r^2} \rho_j c_{sj}^2 \int_0^{w_1} \operatorname{Re} \left[\frac{C_q(u)}{\gamma} (t - \Sigma \alpha_k d_k) \right] w dw \quad (2.14.5)$$

$$Y_{rr}^{sq} = -\frac{8}{\pi r^2} \rho_j c_{sj}^2 \int_0^{w_1} \operatorname{Re} \left[\frac{\alpha_{sj} S_q C_q(u)}{u \gamma} (t - \Sigma \alpha_k d_k) \right] w dw \quad (2.14.6)$$

$$Z_{\phi\phi}^{pq} = \frac{4}{\pi} \rho_j \left(1 - 2c_{sj}^2 / c_{pj}^2 \right) \int_0^{w_1} \operatorname{Re} \left[\frac{C_q(u)}{\gamma} \right] w dw \quad (2.14.7)$$

$$Y_{\phi\phi}^{pq} = -Y_{rr}^{pq} \quad (2.14.8)$$

$$Y_{\phi\phi}^{sq} = -Y_{rr}^{sq} \quad (2.14.9)$$

$$Z_{rz}^{pq} = -\frac{8}{\pi r} \rho_j c_{sj}^2 \int_0^{w_1} \operatorname{Re} \left[\frac{\alpha_{pj} S_q C_q(u)}{\gamma} (t - \Sigma \alpha_k d_k) \right] w dw \quad (2.14.10)$$

$$Z_{rz}^{sq} = \frac{4}{\pi r} \rho_j c_{sj}^2 \int_0^{w_1} \operatorname{Re} \left[\frac{A_j C_q(u)}{u \gamma} (t - \Sigma \alpha_k d_k) \right] w dw \quad (2.14.11)$$

$$Z_{\text{mean}}^{pq} = \frac{4}{\pi} \rho_j \left(1 - \frac{4}{3} c_{sj}^2 / c_{pj}^2 \right) \int_0^{w_1} \operatorname{Re} \left[\frac{C_q(u)}{\gamma} \right] w dw \quad (2.14.12)$$

All Y response functions are zero except Y_{rr}^{pq} , Y_{rr}^{sq} , $Y_{\phi\phi}^{pq}$, and $Y_{\phi\phi}^{sq}$ which are listed above. In addition, Z_{rr}^{sq} , $Z_{\phi\phi}^{sq}$, and Z_{mean}^{sq} are zero.

2.15 LIMITING VALUES OF THE POTENTIAL SOLUTIONS AT $t = t_{2q}$ AND $r = 0$

The case for which $c_{pmin}^{-1} < y_{2max} = c_k^{-1} \sin \theta_k$ corresponds to the supercritical reflection of plane wave theory. This case occurs when $\sin \theta_k > \sin \theta_{\text{crit}} = c_k / c_{pmin}$. It can be shown for the supercritical reflection that the response to a step wave source has a logarithmic singularity at $t = t_{2q}$. However, if the source function and its time derivative vanish more rapidly than a logarithm diverges as $t \rightarrow r/c_{pm}$, the response obtained after convolution is finite.

For subcritical cases ($\sin \theta_k < \sin \theta_{\text{crit}}$) the responses at $t = t_{2q}$ have finite values. The stepwave response functions for the potentials (2.12.5) and (2.12.6), for the velocities (2.13.7)-(2.13.10), and for the stresses (2.14.2)-(2.14.12) can all be written in the form

$$F(t) = \int_0^{w_1} \operatorname{Re} \left[\frac{f(u, t)}{\gamma} \right] w dw \quad (2.15.1)$$

Then using the procedure of Cagniard (1962) pages 88 and 89, the value of F at $t = t_{2q}$ for $r > 0$ is

$$F(t_{2q}) = \frac{\pi}{4} \frac{\text{Im}[f(u, t_{2q})]}{\left[y_{2\max} r \sum_k d_k c_k^{-2} / \alpha_k^3 \right]^{1/2}} \quad (2.15.2)$$

evaluated at $u = iy_{2\max}$ where $y_{2\max}$ and t_{2q} are given by (2.11.1) and (2.11.2), respectively.

In the case $r = 0$, the solutions simplify considerably. The expressions for the potentials can be easily derived by setting $r = 0$ in equations (2.9.1) and (2.9.2) and using $J_0(0) = 1$ and $J_0'(0) = 0$. Equation (2.9.7) reduces to

$$t = \sum_k \alpha_k d_k \quad (2.15.3)$$

and u is real rather than a complex variable. Then making the change of integration variables from u to t as in Section 2.9, the solutions can be inverted to obtain

$$X_{jq}(r=0) = \frac{C_q(u)}{u \sum_k d_k / \alpha_k} \quad (2.15.4)$$

$$U_{jq}(r=0) = 0 \quad (2.15.5)$$

where u is obtained from (2.15.3). The arrival time arguments of Section 2.11 do not apply for $r = 0$. For this case the arrival time is

$$t_{1q} = t_{2q} = \sum_k c_k^{-1} d_k \quad (2.15.6)$$

which results from $u = 0$. In (2.15.4) the limit as $u \rightarrow 0$ of $C_q(u)/u$ must be taken at the arrival time.

The corresponding velocity and stress stepwave responses for a P wave source are of the form

$$F(r = 0) = \frac{\pi}{\Omega} \frac{r(u)}{u \sum_k d_k / \alpha_k} \quad (2.15.7)$$

where the notation of (2.15.1) has been used. Note that all response terms containing $t - \sum_k \alpha_k d_k$ in the numerator vanish at $r = 0$ since this factor results from $J'_0(\text{sur})$ which is zero at $r = 0$. All other velocity and stress component terms involving S waves are also zero at $r = 0$ since they result from U_j and its derivatives.

CHAPTER 3

THE CAGGS CODE

3.1 GENERAL DESCRIPTION

A computer program CAGGS (Cagniard Ground Shock) was written to calculate the particle velocity components v_r and v_z for the three layer (fluid-solid-solid) case where the point source is in the fluid and the receiver is in the finite layer. Displacement calculations obtained by numerically integrating the velocities are also available.¹

The code can calculate up to 183 arrival times which include all rays having 12 or fewer reflections and the $P^{13}P$ ray having 13 reflections. However, reflection and transmission coefficient products RKT are coded for only 71 of the typically earliest arrivals. The available rays are $P - P^6P^3P$, $F^6P - P^3S^3S$, $P^7P - P^5S^2P$, $P^8P - P^6S^2S$, $P^9P - P^8SP$, $P^{10}P - P^9SS$, $P^{11}P - P^{10}SP$, $P^{12}P - P^{11}SS$, and $P^{13}P$. These rays allow calculating velocity-time curves for approximately 3 to 4 S wave transit times of the layer after the first arrival.

The CAGGS code was written in FORTRAN for the Honeywell 600-6000 series computers. The code is run in the time sharing mode from a Tektronix 4014 high speed graphics terminal. Hard copy of the information on the screen is available at the push of a button. The output is a table of velocity and displacement versus time and velocity and displacement history plots such as the calculated curves in Figures 3-10. The curves shown have been reduced to about 1/2 the original size.

3.2 USER INPUTS AND OUTPUTS

Table 2 shows an example calculation including input and tabular output every tenth time step. The decay exponent allows calculations for a $1/r^H$ decay in layer 2. All computations in this report used a pure linear decay with an exponent 1.0. The next input selects which plots are desired. The gate frequency input allows calculation of

¹ A variation of the CAGGS code which calculates stress components in medium 2 is also available.

Table 2. Sample printout of a CAGGS calculation.

```

*****
DECAY EXPONENT IN LAYER 2 (1.0 FOR LINEAR)
*1
PLOTS DESIRED (0=NONE, 1=VELOCITY, 2=VELOCITY GAGE, 3=BOTH)
(4=DISPLACEMENT, 5=DIS AND VEL, 6=DIS AND UC, 7=DIS, VEL, AND UC)
*1
GAGE FREQUENCY (HZ)
*600
*U,V
*E, I, J
*G, GSE, RH02
*3, 55, RH03
*14, 8, 2, 7
*MIN, MGRY
*H, H, P, Z
*400, 6, 48, 2
SITE ALTITUDE (FT), AIR TEMPERATURE (DEG. C)
*6600, 15
R, TA, P, MAX 0.48000000E 02 0.89577304E 01 0.67199233E 02

IR T1 T2 TCONST RU PAIR
2 0.66187E 01 0.89834E 01 0.33453E 01 0.45007E 02 0.74130E 02
1 0.61760E 01 0.61760E 01 0.33453E 01 0.47678E 01 0.44900E 03

DEFAULT DT * 0.22302314E 00
INPUT DT (USE 0. FOR DEFAULT VALUE)
*0

TSTOP
-141

IP, T, UZ, UR, D152, D15R
2 0.61760E 01 0.
10 0.72569E 01 0.75280E 01 0.21617E 00 0.89635E 04 0.23104E 03
20 0.80973E 01 0.54688E 01 0.31628E 01 0.17525E 03 0.50028E 03
30 0.19558E 02 0.26121E 00 0.26889E 00 0.48273E 01 0.23463E 04
40 0.12789E 02 0.27766E 00 0.72420E 01 0.10360E 02 0.29564E 03
50 0.15018E 02 0.40952E 01 0.33820E 01 0.14294E 02 0.32490E 03
60 0.17140E 03 0.85577E 01 0.47635E 01 0.14644E 02 0.22167E 03
70 0.19479E 02 0.18604E 00 0.35385E 01 0.11230E 02 0.12894E 03
80 0.21710E 02 0.95963E 01 0.27038E 01 0.89513E 03 0.63518E 04
90 0.23940E 02 0.78807E 01 0.41811E 01 0.67983E 03 0.28342E 04
100 0.26100E 02 0.62376E 01 0.86700E 00 0.43033E 03 0.18237E 05
110 0.28231E 02 0.46232E 01 0.23245E 02 0.32032E 03 0.23024E 04
120 0.30361E 02 0.27582E 01 0.83468E 03 0.25516E 03 0.27280E 04
130 0.32501E 02 0.20502E 01 0.34226E 05 0.20187E 03 0.28186E 04
140 0.34641E 02 0.14086E 01 0.54400E 07 0.16255E 03 0.27522E 04
150 0.36781E 02 0.10703E 01 0.85868E 03 0.13410E 03 0.26365E 04
160 0.41702E 02 0.49377E 02 0.10180E 02 0.11400E 03 0.23814E 04
170 0.44812E 02 0.22054E 02 0.19918E 02 0.10650E 03 0.21454E 04
180 0.46242E 02 0.22054E 02 0.19918E 02 0.92073E 03 0.19015E 04
190 0.48472E 02 0.14081E 02 0.10557E 02 0.87364E 03 0.16616E 04
200 0.50702E 02 0.30318E 03 0.10097E 02 0.85518E 03 0.14328E 04
210 0.52932E 02 0.50842E 03 0.32833E 03 0.85796E 03 0.12184E 04
220 0.55162E 02 0.10883E 02 0.84000E 03 0.87616E 03 0.10204E 04
230 0.57392E 02 0.14938E 02 0.76894E 03 0.80954E 03 0.84622E 05
240 0.59622E 02 0.17961E 02 0.63965E 03 0.84178E 03 0.67772E 05
NUMBER OF RAYS & TIMES * 0.112250000E 04
*UZMAX, UZMIN, URMAX, URMIN
0.11554755E 00 -0.6177067E 00 0.35729400E 00 -0.41508251E 00
*DZMAX, DZMIN, DRMAX, DRMIN
0.17589402E 03 -0.14378562E 02 0.50028244E 03 -0.34078202E 03
*UZMAX, UZMIN, URMAX, URMIN
0.106581011E 00 -0.55070517E 00 0.30873280E 00 -0.37424532E 00

```

motion records which simulate the response of velocity gages to the theoretical velocity. The variable IW specifies the type of explosive device. $IW = 1$ for nuclear and $IW = 2$ for conventional explosives (H.E.). W is the charge weight in kilotons nuclear or pounds T.N.T. equivalent weight H.E. The next two lines are the wave speeds (ft/msec) and densitites (gm/cm^3) in media 2 and 3. The parameters in the air (medium 1) are not input but are determined by the program from empirical formulae. $NMIN$ and $NRAY$ specify the minimum and maximum values of q to be used. H , h , r , Z are, respectively, the layer thickness, explosive source height of burst, horizontal range, and $-z$ the depth of gage or receiver. These variables are specified in feet. The next two inputs are the site altitude and air temperature used in calculating the airblast.

The first line of output gives the arrival time (msec) and peak overpressure (psi) at $z = 0$ directly above the burst position. The following table gives characteristic parameters for each ray where

- $IR = q$
- $T1 = \text{time of arrival (msec)} \quad t_{1q}$
- $T2 = \text{time of arrival (msec)} \quad t_{2q}$
- $TCNST = \text{time constant } \theta_{1q} \text{ (msec) described later. For the present version of CAGGS the } \theta_{1q} \text{ are the same for all } q.$
- $RW = \text{horizontal distance } r_q \text{ at which the ray enters medium 2}$
- $PAIR = \text{airblast peak overpressure (psi) at range } RW$
- $DEFAULT \text{ DT} = \text{the time step (msec) which is adequate for most runs. With experience larger steps can often be used.}$
- $TSTOP = \text{time (msec) of the end of the calculation. The code presently allows up to 1000 steps and quits automatically if the maximum is reached.}$

The next output is a table containing the step number IP , time t (msec), velocities v_z and v_R (ft/sec), and displacements l_z and l_r (ft). The maximum and minimum values of the velocities, displacements, and the velocities measured by a simulated velocity gage are listed following the table.

All of the input-output described above is printed on the terminal

screen. Hard copy is obtained by pressing the "copy" key. If plots were specified, the user presses the "return" key after the copying is completed. The program clears the screen and draws a plot. The code stops after each plot to allow copying and continues when the "return" key is depressed. After a case is completed the program allows changing all or only part of the input.

3.3 NUMERICAL INTEGRATION PROCEDURE

To obtain particle velocity components v_r and v_z , two numerical integrations must be performed for each ray. First, the stepwave responses must be evaluated from equations (2.13.7)-(2.13.10). Second, the convolution integrals in the form of (2.13.6) must be computed.

To start the calculation, $y_{2\max}$ is computed for each ray from (2.11.1) using the Method of False Position (Conte (1965)) combined with an increment halving iteration scheme to insure convergence in difficult cases. Arrival times t_{1q} and t_{2q} are then determined from (2.11.2) and (2.11.4) as appropriate. The source amplitude and other time independent terms of the step responses are calculated in the same section of the code. The stepwave responses are then evaluated using a four point Gaussian quadrature with eight subintervals for a total of 32 points. The V_r and V_z integrals are calculated together since most of the factors in the integrals are the same. The integration limit \bar{u}_1 is obtained from a Newton's Method iteration (Conte (1965)) for u_1 in (2.10.4). When $t_{1q} < t < t_{2q}$, the substitution $u_1 = -iy_2$ is used to allow calculation with real arithmetic. When $t > t_{2q}$, complex arithmetic must be used in the iteration. In either case, an initial guess based on the value of u_1 from the previous time step generally produces rapid convergence.

The convolution integration is simplified by expressing the source pressure time dependence $P_o(t)$ in the form

$$P_o\left(t - \frac{R}{c_{p1}}\right) = \sum_k a_k e^{-(t-R/c_{p1})/\theta_k} \quad (3.3.1)$$

Because of the property $e^{x+\Delta x} = e^x e^{\Delta x}$, the convolution can be written

$$\begin{aligned} & \int_0^t P'_0(t - \lambda) V(\lambda) d\lambda \\ &= -\sum_k \left(\frac{a_k}{\theta_k} \right) \left[e^{-\Delta t / \theta_k} \int_0^{t-\Delta t} e^{-(t-\Delta t-\lambda)/\theta_k} V(\lambda) d\lambda \right. \\ & \quad \left. + \int_{t-\Delta t}^t e^{-(t-\lambda)/\theta_k} V(\lambda) d\lambda \right] \end{aligned} \quad (3.3.2)$$

if $P_0 = H(t - R/c_{p1}) p(t - R/c_{p1})$ where $P(0) \neq 0$, we must add an additional term to (2.13.6) corresponding to $\frac{d}{dt} H(t - R/c_{p1}) \delta(t - R/c_{p1})$. The result is

$$\int_0^t P'_0(t - \lambda) V(\lambda) d\lambda = p(0) V(t) + \int_0^t p'(t - \lambda) V(\lambda) d\lambda \quad (3.3.3)$$

The last integral can then be expressed as in (3.3.2).

The first integral in (3.3.2) is the convolution from the previous time step multiplied by an exponential. Thus in a time step we must only calculate the second integral. For times not near a singularity time t_{p1} for a supercritical reflection, we integrate as follows. Denote $t_1 = t - \Delta t$ and

$$V_1 = V(t - \Delta t) \quad (3.3.4)$$

$$V_0 = V(t) \quad (3.3.5)$$

Use linear interpolation between the calculated points

$$V = V_1 + (V_2 - V_1)(t - t_1)/\Delta t \quad (3.3.6)$$

then

$$I_2 = \int_{t-\Delta t}^t e^{-(t-\lambda)/\theta_k} V(\lambda) d\lambda \quad (3.3.7)$$

$$= \theta_k \left\{ V_2 - \left(\frac{V_2 - V_1}{\Delta t} \right) \theta_k + \left[\left(\frac{V_2 - V_1}{\Delta t} \right) \theta_k - V_1 \right] e^{-\Delta t/\theta_k} \right\}$$

Near a singularity time t_{2q} we make the change of variable

$$x = |t_{2q} - \lambda|^{1/2} \quad (3.3.8)$$

to eliminate the logarithmic singularity from the integral producing

$$I_2 = \pm 2 \int_{x(t-\Delta t)}^{x(t)} \left[e^{-(t-\lambda)/\theta_k} V(\lambda) \right] x dx \quad (3.3.9)$$

where + and - apply to $t > t_{2q}$ and $t < t_{2q}$, respectively. This integral is evaluated using a generalized Simpson's rule obtained by integrating a parabola fit to $V(t)$, $V(t - \Delta t)$, and $V(t_0)$ where t_0 is the time of the step before $t - \Delta t$. A fixed time step is not required. The convolution integrations (3.3.7) or (3.3.9) take only a small percentage of the computing time required to evaluate the $V(t)$, hence several terms in the sum of (3.3.1) can be used to fit the source time dependence $P_0(t)$ without adding significantly to the total computing time.

3.4 MODELING THE AIRBLAST WAVEFORM

The point source amplitude and waveform used in the CAGGS code was

chosen to simulate the airblast overpressure produced by airburst explosion of spherical charges. Empirical curve fits based on explosive field test data were used. Peak overpressure P_{\max} and arrival time t_a at the air-soil interface ($z = 0$) for height of burst h and horizontal range r were obtained from formulae extracted from the ANSWER (Analysis System for Weapons Effects Research) code (Britt (1980)). The nuclear section uses the Brode (1970, 1978) height of burst curves. The conventional explosive (H.E.) values are based on curves developed for the ANSWER code.

For the ranges of interest for most linear ground shock calculations and for the common surface tangent burst configuration (charge resting on the ground), the H.E. peak overpressure and arrival time curves can be approximated by

$$P_{\max} \approx 3770 \tilde{r}^{-2.57} \text{ psi for } 2.5 \leq \tilde{r} \leq 12 \text{ ft/lb}^{1/3} \quad (3.4.1)$$

$$\tilde{t}_a \approx 0.044 \tilde{r}^{1.95} \text{ msec/lb}^{1/3} \text{ for } 2 \leq \tilde{r} \leq 15 \text{ ft/lb}^{1/3} \quad (3.4.2)$$

where W is the explosive charge weight in pounds T.N.T., $\tilde{r} = r/W^{1/3}$ and $\tilde{t}_a = t_a/W^{1/3}$. The value of P_{\max} given here is that measured at ground level and hence contains both the incident (or source contribution) and the reflection. Because of the great impedance mismatch between the air and soil, the linear theory predicts a reflection virtually identical to the incident pulse if the soil layer is very thick. In order to match the total pressure (normal stress τ_{zz}) at the interface, one half of the empirical blast overpressure is used for the incident pressure in the linear calculations.

The airblast waveforms $P_o(t)$ such as shown in Figure 2 were fit to a sum of exponential terms of equation (3.3.1) using data from the Department of Defense (D.O.D.) explosive tests series given in table 3. The events used in the waveform model were mostly surface tangent bursts supplemented by other near surface detonations. The parameters a_k and θ_k were chosen to fit the experimental parameters noted on Figure 2 as

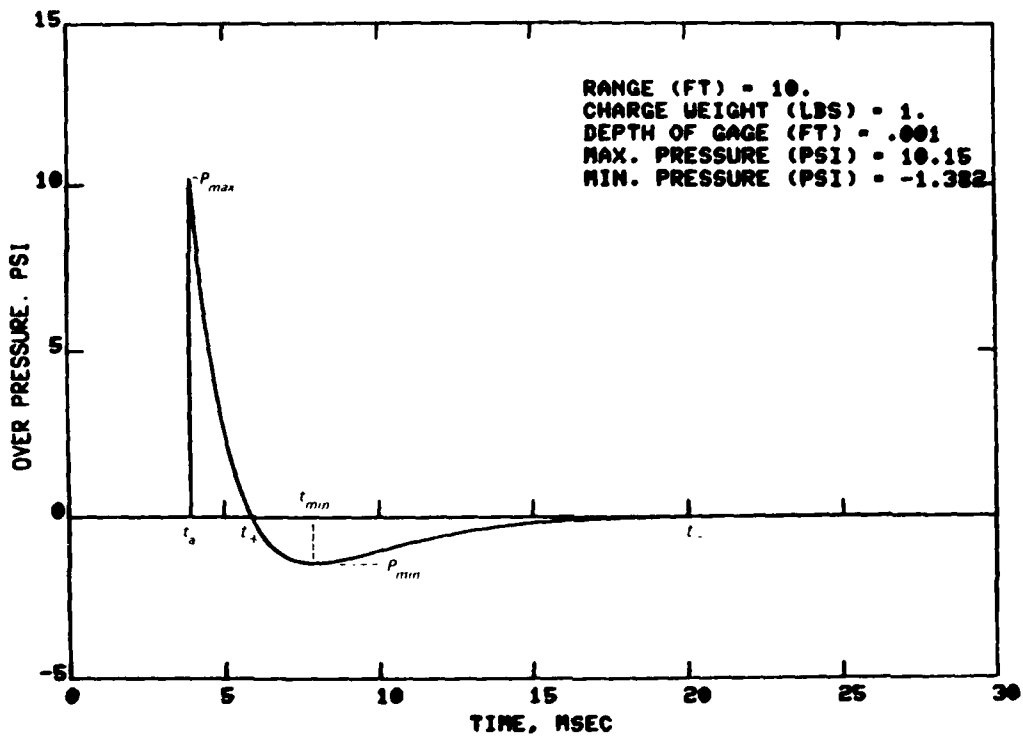


Figure 2 Typical airblast waveform.

Table 3. Explosive test series used in the airblast model.

Test Series	Explosive Charge
CENSE 1	1000 lbs NM ^a
CENSE 2	300 lbs TNT
CENSE 3	200 lbs NM
Dial Pack	500 tons TNT
Mine Ore	100 tons TNT
Mine Under	100 tons TNT
Middle Gust 3	100 tons TNT
Middle Gust 4	100 tons TNT
Mineral Rock	100 tons TNT
Misers Bluff Phase I	1000 lbs TNT
Misers Bluff Phase II	120 tons ANFO ^b
Mixed Company	500 tons, 20 tons TNT
Pre-Dice Throw 11	100 tons TNT, 120 tons ANFO
Pre-Mine Throw IV	1004 lbs TNT, 7.2 tons, 102.4 tons NM
1969 Height-of-Burst Series (BRL)	1000 lbs TNT

NOTE: A table of factors for converting inch-pound units of measurement to metric (SI) units is presented on page 3.

^a Nitromethane (NM)

^b Ammonium nitrate and fuel oil (ANFO)

well as the positive phase impulse I_+ (the integral of the curve from t_a to t_+). A large body of data was obtained from reports on P_{\max} , I_+ , t_a and t_+ . A representative, but much smaller, quantity of information on the negative phase was used. More data was available from the agencies conducting the tests or from D.O.D. archives, but time and funding limitations prohibited the extensive use of this material. The scatter of the data used in determining the negative phase parameters is much greater than for the positive phase. It is expected that the negative phase model used here will not be changed greatly when a larger data base is used.

The resulting waveform for T.N.T. explosions is

$$P_o(\tilde{t}) = P_{\max} e^{-\tilde{t}/\tilde{\theta}_1} + a_2 \left(e^{-\tilde{t}/\tilde{\theta}_2} - e^{-\tilde{t}/\tilde{\theta}_3} \right) + a_4 \left(e^{-\tilde{t}/\tilde{\theta}_4} - e^{-\tilde{t}/\tilde{\theta}_5} \right) \quad (3.4.3)$$

where P_{\max} is the peak overpressure in psi, W is the charge weight in pounds of T.N.T., $\tilde{t} = t/W^{1/3}$ msec/lb^{1/3}, $\tilde{\theta}_k = \theta_k/W^{1/3}$ msec/lb^{1/3},

$$a_2 = \text{minimum} \begin{cases} 200 P_{\max}^{0.48} \\ 4010 \end{cases} \quad (3.4.4)$$

$$a_4 = \begin{cases} 21 P_{\max}^{0.1} & \text{for } 5 \leq P_{\max} \leq 29.1 \text{ psi} \\ 7930 P_{\max}^{-1.66} & \text{for } P_{\max} > 29.1 \text{ psi} \end{cases} \quad (3.4.5)$$

$$\tilde{\theta}_1 = \begin{cases} 6.26 P_{\max}^{-0.69} & \text{for } 5 \leq P_{\max} \leq 200 \text{ psi} \\ 218 P_{\max}^{-1.36} & \text{for } 200 \leq P_{\max} \leq 700 \text{ psi} \\ 0.084 P_{\max}^{-0.16} & \text{for } P_{\max} > 700 \text{ psi} \end{cases} \quad (3.4.6)$$

$$\tilde{\theta}_4 = \begin{cases} 11 P_{\max}^{-0.28} & \text{for } P_{\max} \leq 200 \text{ psi} \\ 2446 P_{\max}^{-0.13} & \text{for } 200 < P_{\max} < 700 \text{ psi} \\ 0.49 & \text{for } P_{\max} \geq 700 \text{ psi} \end{cases} \quad (3.4.7)$$

$$\tilde{\theta}_2 = \text{minimum} \begin{cases} 0.5 \tilde{\theta}_4 \\ 5.6 P_{\max}^{-0.38} \end{cases} \quad (3.4.8)$$

$$\tilde{\theta}_3 = 0.99 \tilde{\theta}_2 \quad (3.4.9)$$

$$\tilde{\theta}_5 = 1.01 \tilde{\theta}_4 \quad (3.4.10)$$

A finite rise time can be introduced by adding an additional term to (3.4.3) of the form $a_6 e^{-t/\tilde{\theta}_6}$, where

$$a_6 = -a_1 \quad (3.4.11)$$

Let $\tilde{\Delta t}_0$ be the scaled rise time of the pulse, then if the last four terms of (3.4.3) change only slightly in this time, $\tilde{\theta}_6$ can be approximated by

$$\frac{\tilde{\Delta t}_0}{\tilde{\theta}_1} \approx \frac{\ln\left(\frac{\tilde{\theta}_1}{\tilde{\theta}_6}\right)}{\frac{\tilde{\theta}_1}{\tilde{\theta}_6} - 1} \quad (3.4.12)$$

The amplitude P_{\max} of $P_0(t)$ is then obtained by replacing $a_1 = P_{\max}$ by

$$a_1 = \frac{P_{\max}}{e^{-\tilde{\Delta t}_0/\tilde{\theta}_1} - e^{-\tilde{\Delta t}_0/\tilde{\theta}_6}} \quad (3.4.13)$$

3.5 APPROXIMATION OF THE AIRBLAST WITH A POINT SOURCE

As can be seen from the empirical formulae described above, the airblast cannot be directly modeled as a linear point source in our range of interest ($10 \leq P_{\max} \leq 200$ psi) since (a) the airblast peak overpressure decays like $1/R^{2.57}$ instead of $1/R$, (b) the blast propagation rate decreases with range instead of the constant speed c_{pl} , and (c) the shape of the waveform changes with range rather than being a fixed function $P_o(t - R/c_{pl})$. Within the framework of the Cagniard model two options are available for approximating the empirical airblast: (a) simulating the pressure in space and time by a distribution of point sources or (b) using a single point source chosen to linearize around a particular range related to the time of dominant motion. The first option would be more accurate but would likely require much more computer time to evaluate. The simpler and less costly linearization approach (b) was used in this study. Several procedures were investigated, but linearization around ray $q = 2$, the directly transmitted shear wave (path A of Figure 1), produced the best overall agreement with measured velocity waveforms for materials ranging from weak soils to hard rock.

The directly transmitted S wave path was determined by iterating for the range r_s at which the ray enters the soil. The empirical formulae (such as (3.4.2)) were used to calculate the blast arrival time t_a for an initial value of $r_s = r$. An average P wave speed c_{pl} in the air was computed from

$$c_{pl} = \frac{\left(h^2 + r_s^2\right)^{1/2}}{t_a} \quad (3.5.1)$$

Then from equations (2.11.2) and (2.11.3) we obtained the relations

$$t_a = \left(c_{pl}^{-2} - y_{2\max}^2\right)^{1/2} h + \left(c_{s2}^{-2} - y_{2\max}^2\right)^{1/2} z + y_{2\max} r_s = 0 \quad (3.5.2)$$

$$y_{2\max} = \frac{c_{pl}^{-1} r_s}{\left(h^2 + r_s^2\right)^{1/2}} \quad (3.5.3)$$

which must also be satisfied for the ray. These equations are actually a disguised statement of Snell's Law of Refraction. Using the initial values of r_s and c_{pl} in (3.5.2) and (3.5.3) a new estimate of r_s was obtained. It is easily seen that the solution lies between r and this second estimate of r_s . Hence, iteration was continued using an interval halving technique on this interval until (3.5.1)-(3.5.3) were satisfied within an acceptable tolerance. The point source amplitude and pulse shape were then chosen using the empirical formulae to match the airblast at the point $(r_s, 0)$. The resulting c_{pl} and point source function $P_0(t - R/c_{pl})/R$ were then used for all the rays.

CHAPTER 4

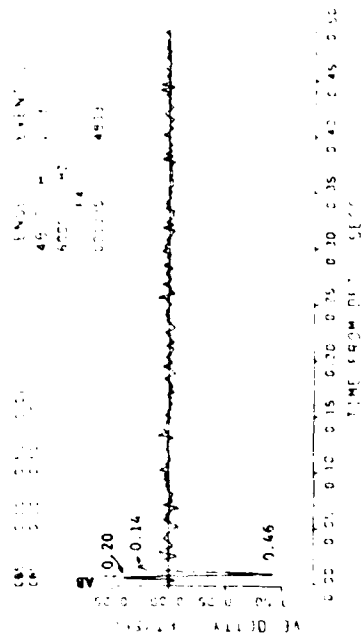
COMPARISON OF CALCULATED AND MEASURED PARTICLE VELOCITY WAVEFORMS

4.1 SELECTION OF TEST SERIES

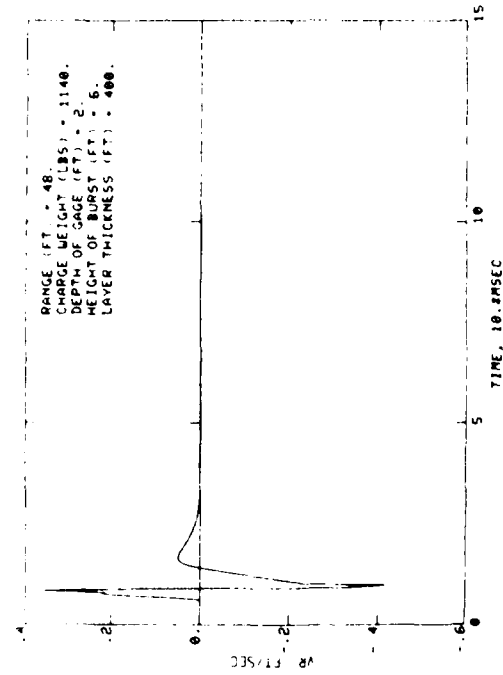
Calculations were performed for the three CENSE (Coupling Efficiency of Near Surface Explosions) explosive field test series (in years 1977, 1980). These tests were chosen because they provide a variety of site characteristics which were relatively well controlled. The test beds were either effectively homogeneous or had layering suitable for the two-layer model. In addition, each of the series had near surface airburst explosions for which particle velocity or acceleration was measured in the upper layer for a variety of ranges from the explosions.

4.2 CALCULATIONS FOR CENSE 1

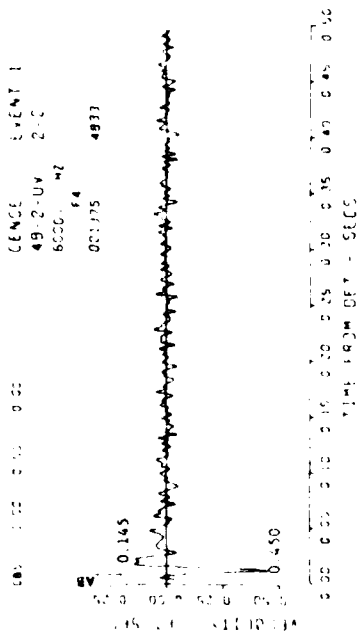
CENSE 1 consisted of a series of 1000-lb spheres of nitromethane (1140 lbs TNT equivalent) detonated over a massive Kayenta sandstone formation. These events provide data for checking the calculations for motion in a strong, homogeneous material which behaves elastically for stress levels of hundreds of psi. The surface rock was thick enough that three layers were not needed for the computations. Figure 3 compares the theoretical and measured vertical and radial velocity components. Vertical velocity is positive for upward motion and radial velocity is positive for outward motion. Note that the experimental and theoretical curves are plotted on different scales and that the calculation represents only part of the measured curve. The material properties used for this calculation were $\rho_1 = 0.0012 \text{ gm/cm}^3$, $c_{p2} = 9 \text{ ft/msec}$, $c_{p1} = 4 \text{ ft/msec}$ and $\rho_2 = 2.4 \text{ gm/cm}^3$. Event 1, shown in the figure, was detonated with its charge center 6 ft above the rock. Measurements were made with velocity gauges (having a nominal 600-Hz frequency response) placed 2 ft below the rock surface. The airblast peak pressure above the gauge was measured at 51 psi at the



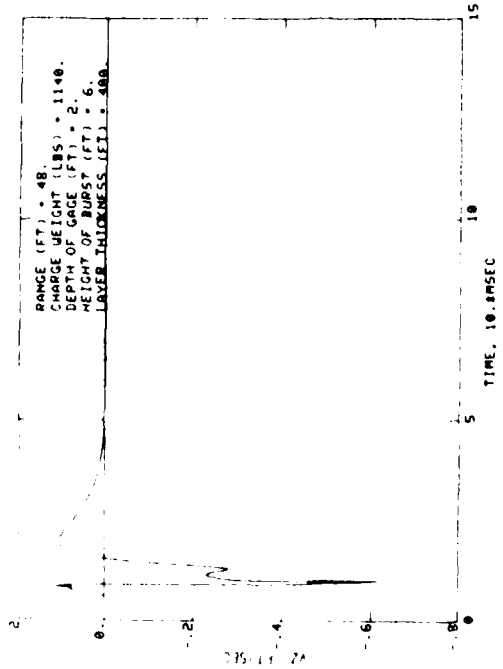
b. MEASURED RADIAL



d. THEORETICAL RADIAL



a. MEASURED VERTICAL



c. THEORETICAL VERTICAL

Figure 3 Comparison of particle velocity calculations with CENSE 1 measurements at 48-ft range.

48 ft range. Figure 4 shows a calculation at the 36-ft range (120 psi). Only the horizontal velocity record was obtained. There is good agreement between calculations and experiment at both ranges except in the magnitude of the second positive phases. This slight discrepancy is probably a result of the simple source linearization and not an effect of non-linear material properties of the rock.

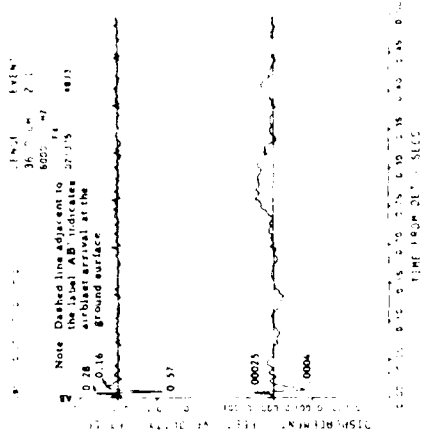
4.3 CALCULATIONS FOR CENSE 2

The data of CENSE 2 provided information to check the elastic calculations for a two-layered clayey-silt soil site. The explosives used were 300-lb spherical TNT charges. In the calculations shown in Figures 5 and 6, the soil was modeled in two layers: a surface layer 20 ft thick with $c_{p2} = 1.1$ ft/msec, $c_{s2} = 0.6$ ft/msec, and $\rho_2 = 1.7$ gm/cm³, and a lower half-space with $c_{p3} = 1.6$ ft/msec, $c_{s3} = 0.7$ ft/msec, and $\rho_3 = 1.75$ gm/cm³. The measurements were made with velocity gages located 1.5 ft below the surface. Event 2 was detonated with charge center 7.2 ft above the soil surface. Excellent agreement was obtained in Figure 5 at the 57-ft (13-psi) range. Figure 6 at the 43-ft (34-psi) range shows slightly poorer agreement but still within typical scatter of field measurements. At a range of 32 ft (60 psi), Figure 7, the linear calculations begin to fail to reproduce the major characteristics of the measured motion. In this case the linear theory does not predict the large initial downward and outward displacements (area under the velocity curve) seen in the experiments. These differences are probably a result of the nonlinear material properties of the soil becoming important and a result of the close-in source conditions not being adequately modeled by the localized airblast input used in the calculations.

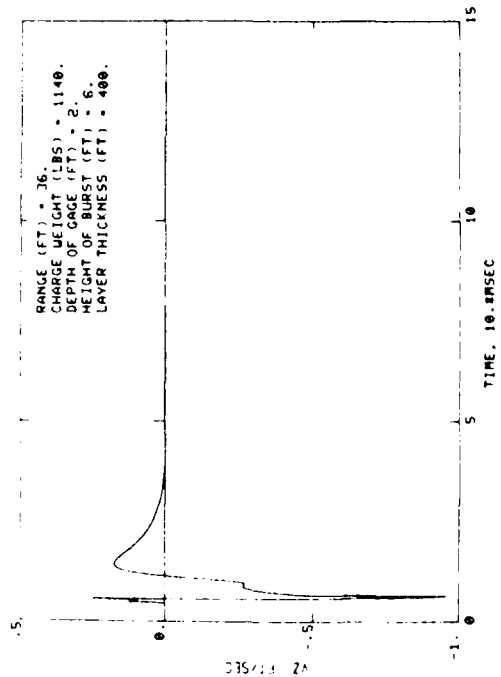
4.4 CALCULATIONS FOR CENSE 3

CENSE 3 provided measurements for comparison with theory for a weak soil layer over a hard rock site. This series consisted of seven explosions of 200 lb (226 lb TNT equivalent) of nitromethane. The test bed consisted of compacted backfill of "alluvium" soil placed over a

NOT AVAILABLE

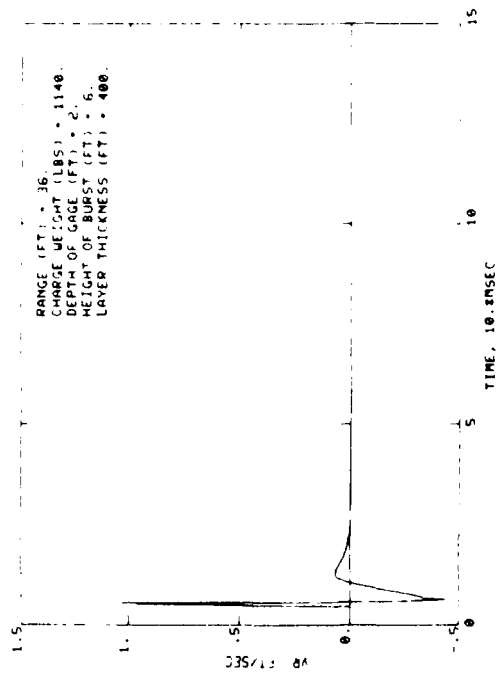


a. MEASURED VERTICAL



c. THEORETICAL VERTICAL

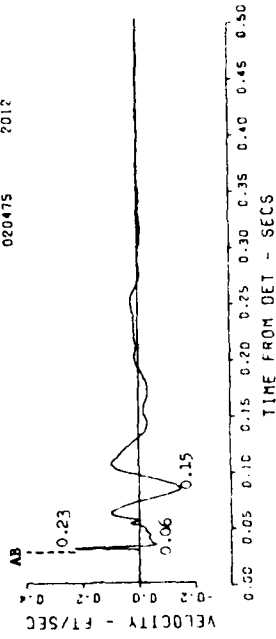
b. MEASURED RADIAL



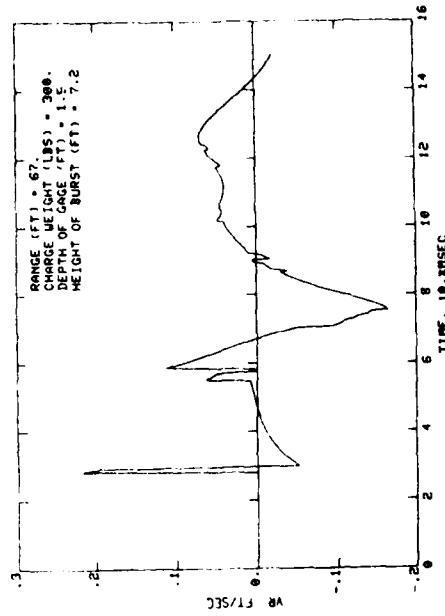
d. THEORETICAL RADIAL

Figure 4 Comparison of particle velocity calculations with CEMSE 1 measurements at 36-ft range.

CENSE-2 EVENT 2
 67-1.5-UH 29
 6000. MZ
 020475 2012

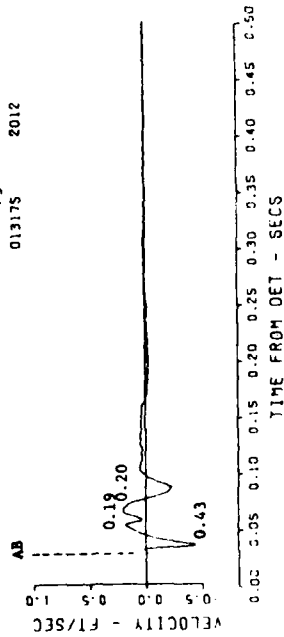


b. MEASURED RADIAL

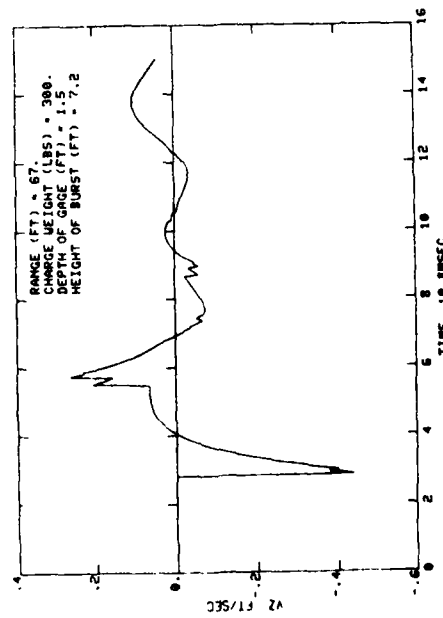


d. THEORETICAL RADIAL

CENSE-2 EVENT 2
 67-1.5-UV 11
 6000. MZ
 F3
 013175 2012



a. MEASURED VERTICAL



c. THEORETICAL VERTICAL

Figure 5 Comparison of particle velocity calculations with CENSE 2 measurements at 67-ft range.

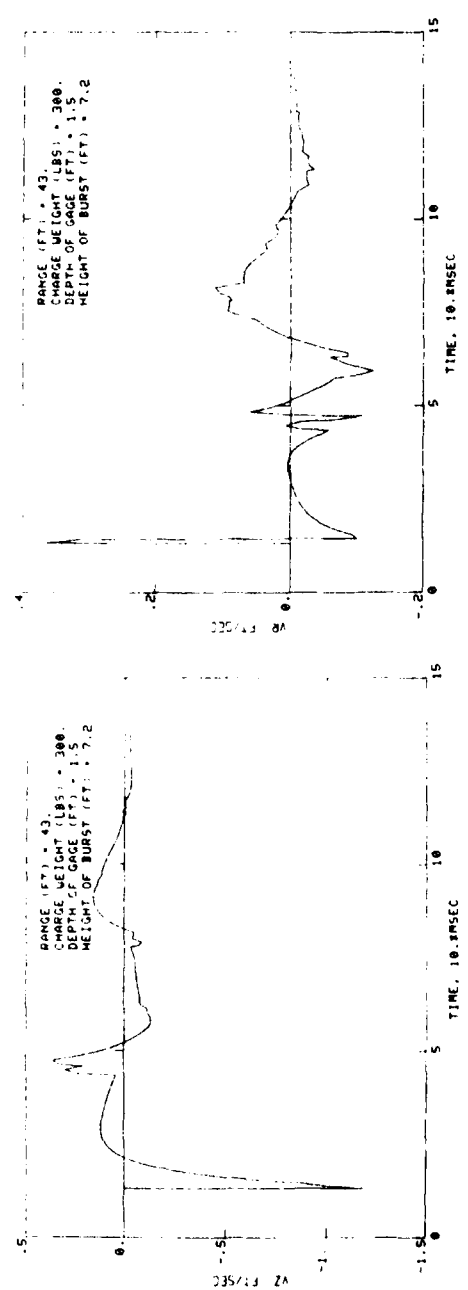
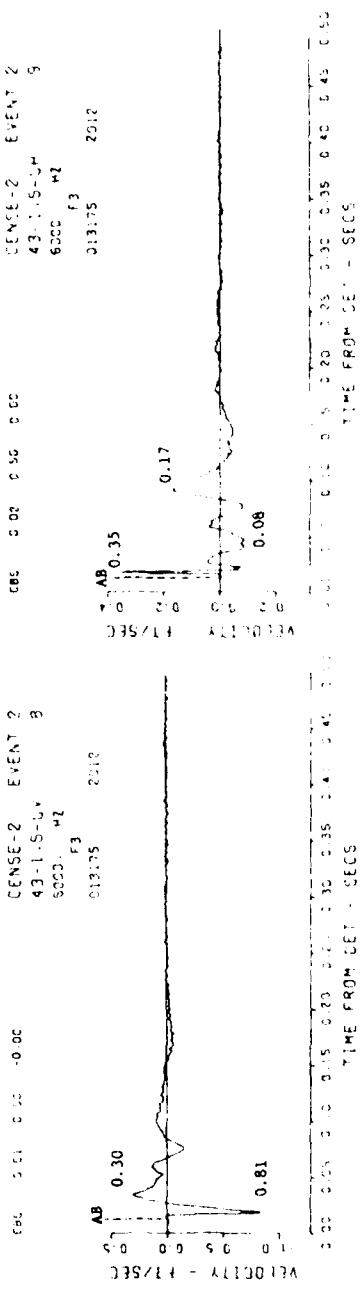
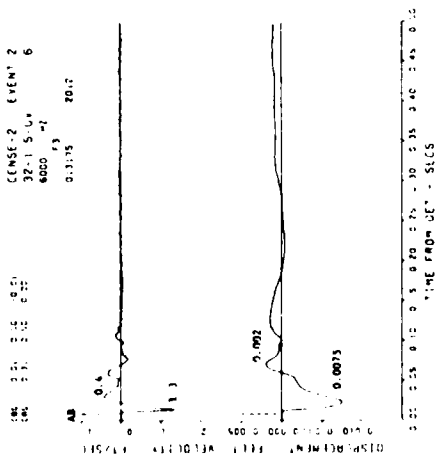
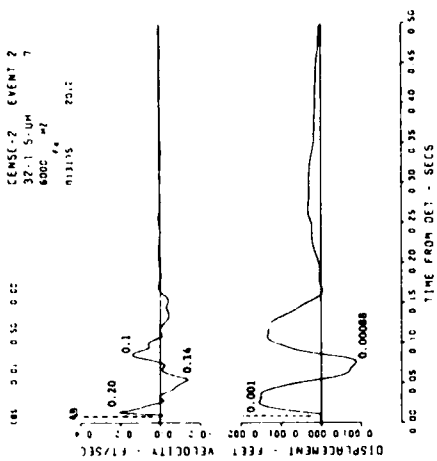


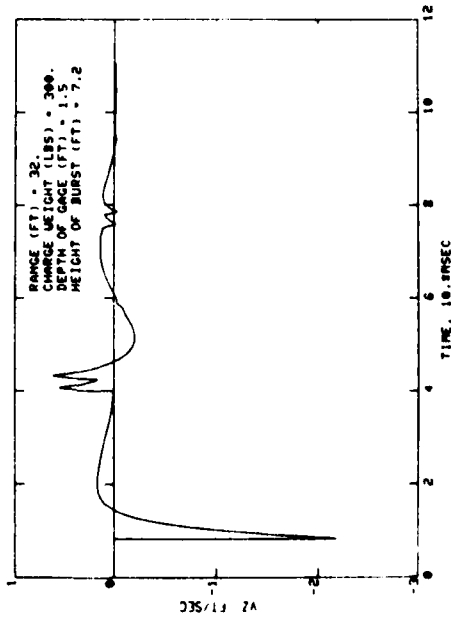
Figure 6 Comparison of particle velocity calculations with CENSE 2 measurements at 43-ft range.



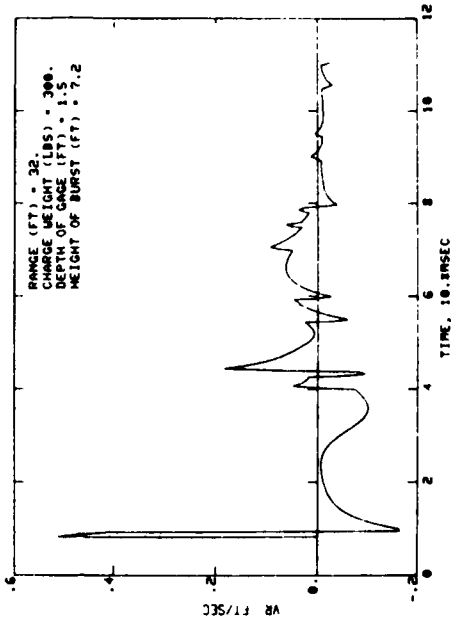
a. MEASURED VERTICAL



b. MEASURED RADIAL



c. THEORETICAL VERTICAL



d. THEORETICAL RADIAL

Figure 7 Comparison of particle velocity calculations with CENSE 2 measurements at 32-ft range.

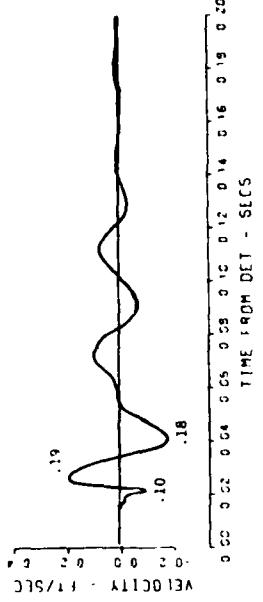
Kayenta sandstone deposit similar to that of CENSE 1. The thickness of the soil was varied from 0 to 6 ft. Measurements of vertical and radial acceleration were made at middepth in the soil layers and in the rock. Velocity histories were obtained by integrating the acceleration records. Events 2 and 4 were surface tangent bursts, that is, the explosive charge was resting on the soil surface. The soil layer thickness in Figure 8 was 6 ft. In Figure 9 the thickness was 3 ft. The material properties used in the calculations were $c_{p2} = 0.9$ ft/msec, $c_{s2} = 0.3$ ft/msec, and $\rho_2 = 1.6$ gm/cm³ for the soil and $c_{p3} = 8$ ft/msec, $c_{s3} = 3$ ft/msec, and $\rho_3 = 2.4$ gm/cm³ for the sandstone.

At the 56-ft (12-psi) range of Figure 8 the calculations are in good agreement with the experimental curves up to a time of about 45 msec if the high frequency spikes are neglected. These spikes result from using an airblast pulse with zero rise time and reflections at a perfectly distinct interface. High frequency motion of this type is filtered out of the measurements because of the nonlinear effects of the soil and finite frequency response of the gages and recording system. At the 32-ft (52-psi) range of Figure 9 agreement is poorer but the initial velocity amplitudes are still close to the measured values. At a range of 24 ft (110 psi) not shown the calculated initial peaks are nearly a factor or two higher than the experimental.

Figure 10 is presented for comparison with Figure 9 to illustrate the effect of further increasing the soil layer thickness at the CENSE 3 site. The initial portions of the records are produced by the directly transmitted P and S waves and are not dependent on the soil thickness. The later motion is a complicated interaction of reflected waves for moderate layer thickness. In going from a layer thickness of 3 ft as in Figure 8 to the 6-ft layer in Figure 9 the change in frequency of the motion is roughly proportional to the layer thickness change, but the waveforms at 12-ft thickness do not follow this pattern.

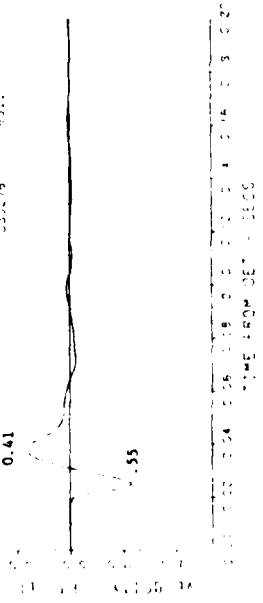
From the few waveforms presented here, one cannot draw general conclusions on factors affecting the period and amplitude of the low frequency motion. A detailed parameter study and analysis will be necessary to determine how the motion changes in going from very thin to very

CENSE-3 EVENT 2 41
 52-56-3-RH 2-12
 12000 HZ
 012075 5311

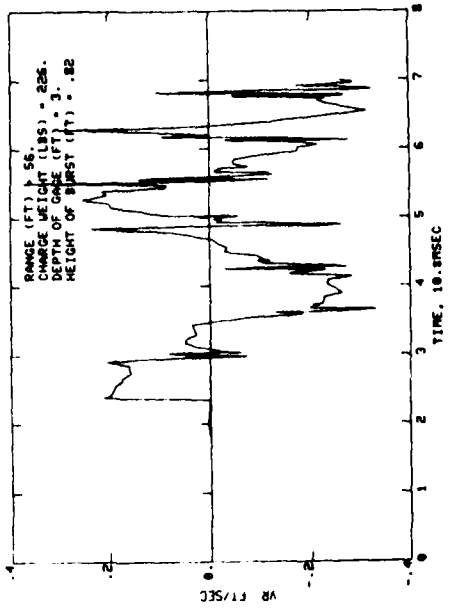


b. MEASURED RADIAL

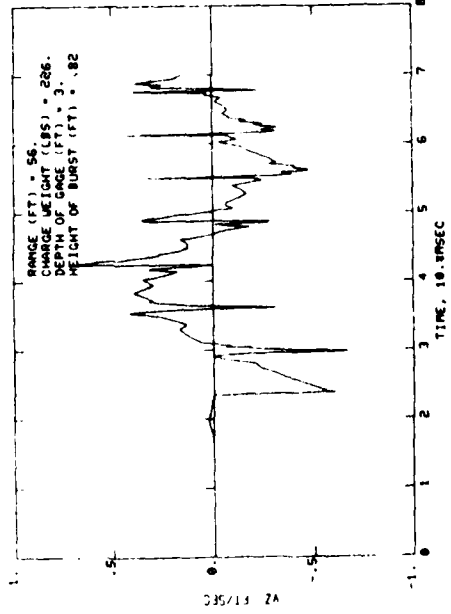
CENSE-3 EVENT 2 40
 52-56-3-RV 2-11
 12000 HZ
 030375 5311



a. MEASURED VERTICAL



d. THEORETICAL RADIAL



c. THEORETICAL VERTICAL

Figure 3 Comparison of particle velocity calculations with CENSE 3 measurements at 56-ft range.

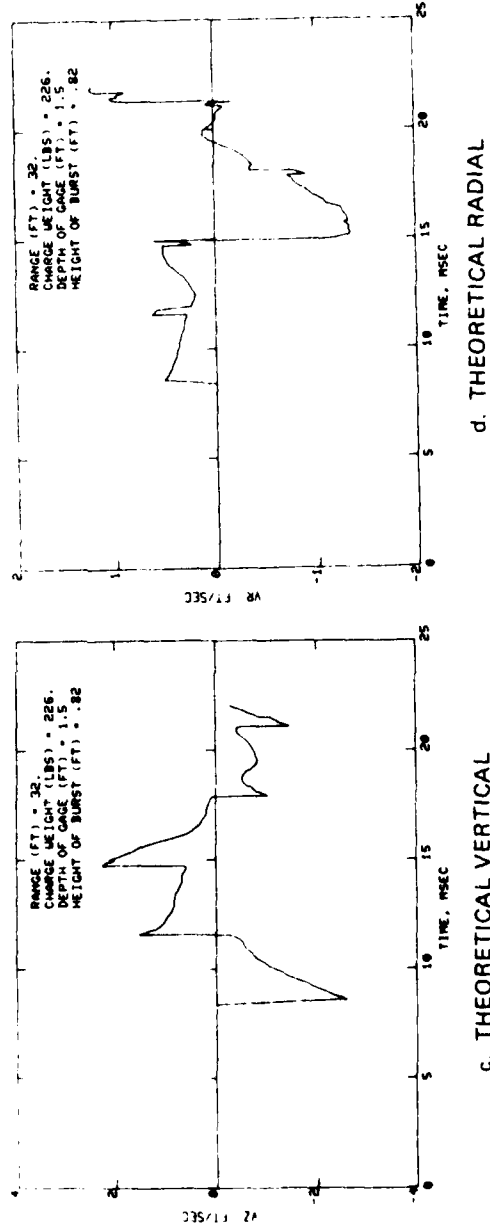
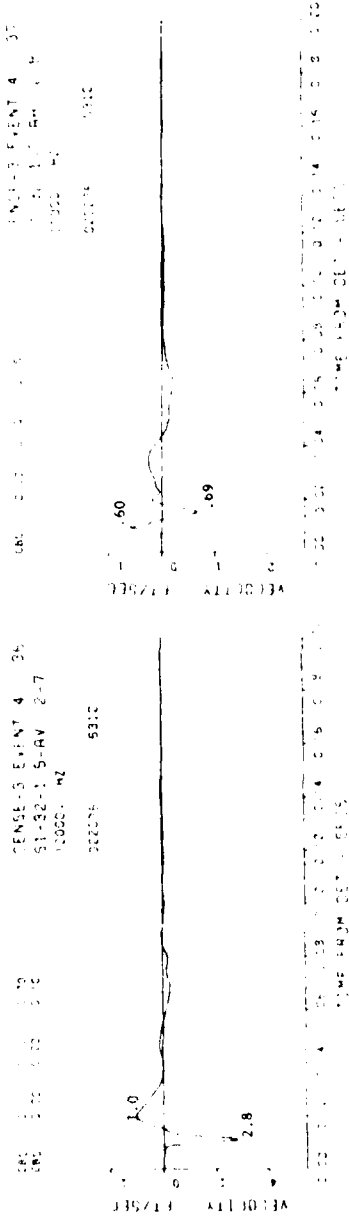
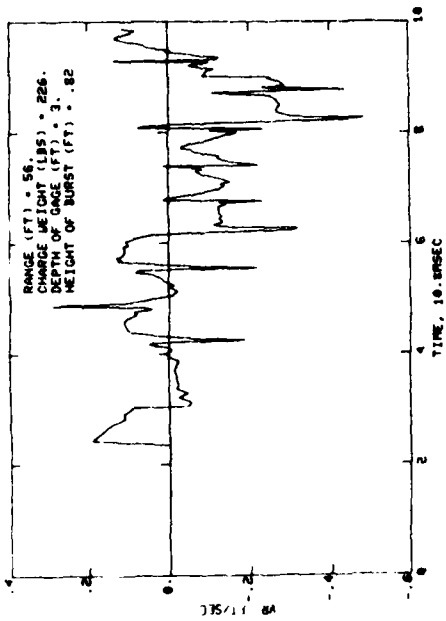
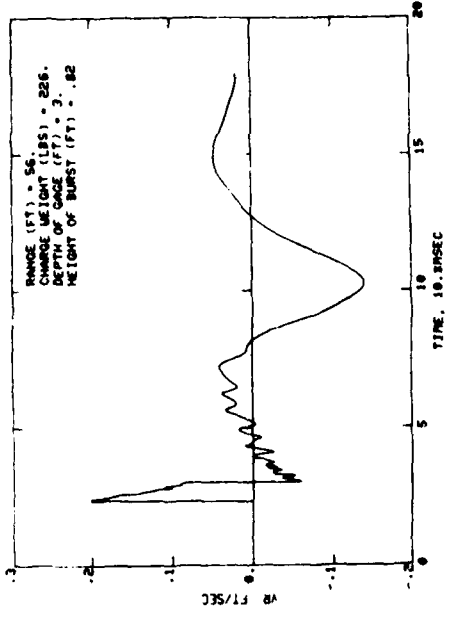
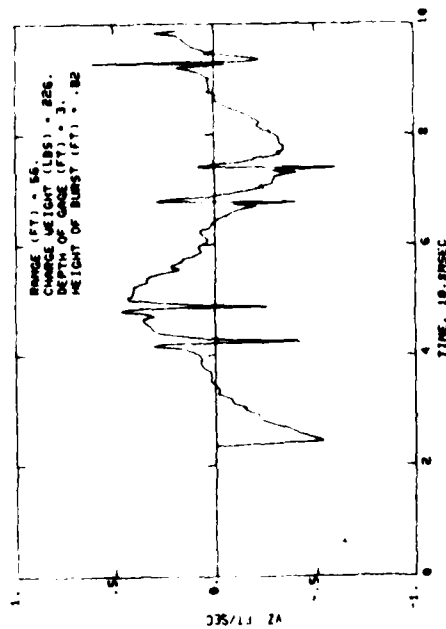


Figure 9 Comparison of particle velocity calculations with CENSE 3 measurements at 32-ft range.



a. VERTICAL, THICK LAYER

b. RADIAL, H = 12 FT



c. VERTICAL, THICK LAYER

d. RADIAL, THICK LAYER

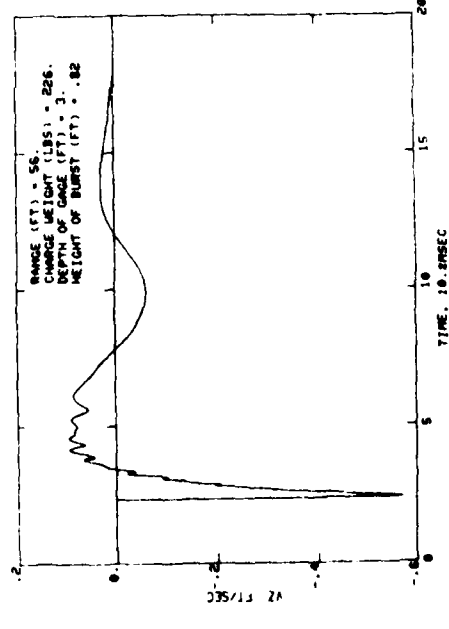


Figure 10 Particle velocity calculations for 12-ft and infinitely thick soil layers.

thick layers. It appears that simple rules of thumb based on S or P wave layer transit times will be valid in only very restricted ranges of thickness and elastic parameters.

CHAPTER 5

CONCLUSIONS AND RECOMMENDATIONS

Calculations performed with the CAGGS code were in *good agreement* with measurements from the three CENSE test series which had very different site conditions and particle velocity waveforms. These sites span much of the spectrum of typical soil-rock environments. CENSE 1 site was a hard, strong, thick sandstone rock; CENSE 2 site was a two layered soil medium; CENSE 3 site was a layer of weak soil backfill over a thick sandstone formation. Based on these calculations, we conclude that predictions of velocity waveforms using the Cagniard formulation of the elastic theory and the localized airblast source model can be expected to be accurate within the scatter of explosive tests measurements for times up to about one cycle of the low frequency motion and for airblast overpressure levels at the gage range up to approximately 40 psi for explosions over weak soils and over 100 psi for strong rocks. At pressure levels in the range of 40 to 100 psi for explosions over soil, the elastic theory still predicts the general character of the motion but overestimates the peak velocities and underestimates the large initial downward and outward displacements.

The simple localized airblast source model linearized around the directly transmitted shear wave may be a major contribution to failure of the calculations at higher pressures and at late time on waveforms. Future work should be directed at improving the source formulation, but any model other than a single point source would greatly increase the computer time costs of the calculations.

The linear wave propagation model can produce motion waveforms for homogeneous sites such as the CENSE 1 sandstone for very small computer costs. But because of the rapidly increasing effort required to calculate the late time portion of waveforms for layered media, routine calculations to times greater than about three shear wave transit times of the layer appear to be more expensive than comparable linear finite difference methods or normal modes techniques. Calculations with the Cagniard theory for more than two soil layers appear to be quite

expensive except for early time motion or special cases where reflections in one layer can be neglected or modeled by a few rays. Our incomplete calculations have indicated that three solid-layer cases such as present at the Dial Pack site where a shallow water table exists with a much deeper rock layer can be effectively modeled by the Cagniard method using only a few carefully selected rays in the thin surface layer.

The primary applications of the CAGGS code for computing motion waveforms in layered media appear to be early time motions up to about two shear wave transit times. These cases require relatively low computing costs and minimal effort to change code inputs. Runs to later times and for more than three layers are practical but are considerably more expensive. Since the theory follows rays, the composite waveforms can be dissected to study the contributions of individual arrivals. This property of the method makes it ideal for studying the basic characteristics and effects of the controlling parameters of wave propagation in layered media. The CAGGS code developed in this study appears to be an ideal tool for performing detailed parametric studies of ground shock at intermediate ranges where the airblast pressure is from 5 to 50 psi in weak soils and to hundreds of psi for strong rock.

REFERENCES

- Abramovici, F. 1970. "Numerical Seismograms for a Layered Elastic Solid," Bulletin of the Seismological Society of America, Vol. 60, pp 1861-1876.
- Abramovici, F. 1978. "A Generalization of the Cagniard Method," J. Comp. Phys., Vol. 29, pp 328-343.
- Abramovici, F. and Alterman, Z. 1965. "Computation Pertaining to the Problem of Propagation of a Seismic Pulse in a Layered Solid," Methods of Computational Physics, Vol. 4, pp 349-379, Academic Press, New York.
- Abramovici, F. and Gal-Ezer, J. 1978. "Numerical Seismograms for a Vertical Point-Force in a Layered Solid," Bulletin of the Seismological Society of America, Vol. 68, pp 81-101.
- Abramovici, F. and Gal-Ezer, J. 1979. "Seismic Waves from Finite Faults in Layered Media," Bulletin of the Seismological Society of America, Vol. 69, pp 1693-1714.
- Brekhovskikh, L. M. 1960. Waves in Layered Media, Academic Press, New York.
- Britt, J. R. 1969. "Linear Theory of Bottom Reflections," NOLTR 69-44, Naval Ordnance Laboratory, Silver Spring, MD.
- Britt, J. R. 1970. "A Solution of the System of Partial Differential Equations Which Describe the Propagation of Acoustic Pulses in Layered Fluid Media," NOLTR 70-234, Naval Ordnance Laboratory, Silver Spring, MD.
- Britt, J. R. 1980. "ANSWER (Analysis System for Weapons Effects Research) Users Manual," Miscellaneous Paper, Army Engineer Waterways Experiment Station, Vicksburg, MS, (in preparation).
- Britt, J. R. and Snay, H. G. 1971. "Bottom Reflection of Underwater Explosion Shock Waves, Computer Program," NOLTR 71-110, Naval Ordnance Laboratory, Silver Spring, MD.
- Brode, H. L. 1970. "Height of Burst Effects at High Overpressures," RM-6301-DASA (DASA 2506), The Rand Corporation, Santa Monica, CA.
- Brode, H. L. 1978. "Improvements and Corrections to DASA 2506, "Height of Burst Effects at High Overpressures", " Letter dated 12 December 1978, R and D Associates, Marina del Rey, CA.
- Cagniard, L. 1939. Reflexion et Refraction des Ondes Seismiques Progressives, Gauthier-Villars, Paris.
- Cagniard, L. 1962. Reflection and Refraction of Progressive Seismic Waves, McGraw-Hill, New York, (translated by E. A. Flinn and C. H. Dix).
- Conte, S. D. 1965. Elementary Numerical Analysis, McGraw-Hill, New York.
- Ewing, W. M., Jardetzky, W. S., and Press, F. 1957. Elastic Waves in Layered Media, McGraw-Hill, New York.

- Ingram, J. K. 1977. "CENSE Explosion Test Program, Report 1, CENSE 1, Explosions in Sandstone, Report 2, CENSE 2, Explosions in Soil," TR N-77-6, Army Engineer Waterways Experiment Station, Vicksburg, MS.
- Ingram, J. K. 1980. "CENSE Explosion Test Program, Report 3, CENSE 3, Explosions in Soil over Sandstone," Technical Report, Army Engineer Waterways Experiment Station, Vicksburg, MS, (in preparation).
- Longman, I. M. 1961. "Solution of an Integral Equation Occurring in the Study of Certain Wave-Propagation Problems in Layered Media," Journal of the Acoustical Society of America, Vol. 33, pp 954-958.
- Fekeris, C. L., Alterman, Z., Abramovici, F. and Jarosch, H. 1965. "Propagation of a Compressional Pulse in a Layered Solid," Reviews of Geophysics, Vol. 3, pp 25-47.
- Pao, Y., Gajewski, R. R., and Stephen, A. T. 1971. "Analysis of Ground Wave Propagation in Layered Media," DASA 2697, Cornell University, Ithaca, NY.
- Pao, Y. and Gajewski, R. R. 1977. "The Generalized Ray Theory and Transient Responses of Layered Elastic Solids," Physical Acoustics, Principles and Methods, Vol. 13, pp 183-265, Academic Press, New York.
- Pao, Y., Gajewski, R. R., and Ceranoglu, A. N. 1979. "Acoustic Emission and Transient Waves in an Elastic Plate," Journal Acoustical Society of America, Vol. 65, pp 96-105.
- Rosenbaum, J. H. 1956. "Shockwave Propagation in Shallow Water I," NAVORD Report 4353, Naval Ordnance Laboratory, Silver Spring, MD.
- Spencer, T. W. 1960. "The Method of Generalized Reflection and Transmission Coefficients," Geophysics, Vol. 25, pp 625-641.
- Spencer, T. W. 1965. "Long-Time Response Predicted by Exact Elastic Ray Theory," Geophysics, Vol. 30, pp 363-368.

In accordance with letter from DAEN-RDC, DAEN-ASI dated 22 July 1977, Subject: Facsimile Catalog Cards for Laboratory Technical Publications, a facsimile catalog card in Library of Congress MARC format is reproduced below.

Britt, James H.

Calculation of ground shock motion produced by airburst explosions using Cagniard elastic propagation theory / by J. H. Britt. Vicksburg, Miss. : U. S. Waterways Experiment Station ; Springfield, Va. : available from National Technical Information Service, 1980.

1, 62 p. : ill. ; 27 cm. (Miscellaneous paper - U. S. Army Engineer Waterways Experiment Station ; SL-80-12)

Prepared for Assistant Secretary of the Army (R&D), Washington, D. C., under Project No. 4A161101A91E.

References: p. 61-62.

1. Air blast waves. 2. Cagniard's method. 3. Computer codes. 4. Elastic waves. 5. Ground motion. 6. Ground shock. 7. Spherical waves. 8. Surface explosions.
I. United States. Assistant Secretary of the Army (Research and Development). II. Series: United States. Waterways Experiment Station, Vicksburg, Miss. Miscellaneous paper ; SL-80-12.
TA7.W34m no. SL-80-12

LMED
18